Neutron reflectometry to investigate the delivery of lipids and DNA to interfaces (Review)

Tommy Nylander
Physical Chemistry 1, Lund University, Box 124, SE-221 00 Lund, Sweden

Richard A. Campbell
Institut Laue-Langevin, BP 156, 38042 Grenoble Cedex 9, France

Pauline Vandoolaeghe
Physical Chemistry 1, Lund University, Box 124, SE-221 00 Lund, Sweden

Marité Cárdenas
Biomedical Technology Laboratory, Faculty of Health and Society, Malmö University, SE-205 06 Malmö, Sweden

Per Linse
Physical Chemistry 1, Lund University, Box 124, SE-221 00 Lund, Sweden

Adrian R. Rennie
Department of Physics, Uppsala University, Box 530, SE-751 21 Uppsala, Sweden

(Received 6 May 2008; accepted 1 August 2008; published 19 December 2008)

The application of scattering methods in the study of biological and biomedical problems is a field of research that is currently experiencing fast growth. In particular, neutron reflectometry (NR) is a technique that is becoming progressively more widespread, as indicated by the current commissioning of several new reflectometers worldwide. NR is valuable for the characterization of biomolecules at interfaces due to its capability to provide quantitative structural and compositional information on relevant molecular length scales. Recent years have seen an increasing number of applications of NR to problems related to drug and gene delivery. We start our review by summarizing the experimental methodology of the technique with reference to the description of biological liquid interfaces. Various methods for the interpretation of data are then discussed, including a new approach based on the lattice mean-field theory to help characterize stimulus-responsive surfaces relevant to drug delivery function. Recent progress in the subject area is reviewed in terms of NR studies relevant to the delivery of lipids and DNA to surfaces. Lastly, we discuss two case studies to exemplify practical features of NR that are exploited in combination with complementary techniques. The first case concerns the interactions of lipid-based cubic phase nanoparticles with model membranes (a drug delivery application), and the second case concerns DNA compaction at surfaces and in the bulk solution (a gene delivery application). © *2008 American Vacuum Society.* [DOI: 10.1116/1.2976448]

I. INTRODUCTION TO NEUTRON REFLECTOMETRY

A. Experimental methodology

Neutron reflectometry (NR) is a fast growing technique that involves the measurement of the specular reflection of neutrons at a planar surface. A well collimated beam of neutrons impinges on a macroscopic smooth interface at a grazing angle of incidence, and the intensity of the reflected beam is measured as a function of either angle or wavelength. The specular reflection, where the angle of the reflected beam is equal to that of the incident beam, provides information about the structure and composition of thin layers in the direction perpendicular to the interface.[1] This information is derived via the nuclear property of scattering length density, which depends on the molecular and isotopic compositions of the bulk materials and interfacial layers.[2] In contrast to the reflection of light at surfaces, which depends on the optical refractive index profile normal to the interface, the isotopes hydrogen (^{1}H) and deuterium (^{2}H or D) have very different scattering properties for neutrons. This facet of neutron scattering means that, through chemical or biological synthesis, the contrast of materials can be enhanced by deuteration of molecular entities or subentities.[3] Furthermore, for liquid interfaces the same layer can be measured with respect to different isotopic contrasts of the solvent, such as water (H_2O), heavy water (D_2O), or a defined mixture of the two solvents to match the scattering properties of the incident medium (e.g., air or silicon).[4] As a result, the same chemical or biochemical environment can be created with different scattering environments, which leads to the acquisition of multiple scattering profiles that can be fitted to a sophisticated structural model of the interface.[5]

The practical aspects of NR are described elsewhere (e.g., in Refs. 2 and 6); however, here we give a brief synopsis of some important points. The ratio of the intensity of the specularly reflected beam to that of the incident beam is measured as a function of either wavelength λ or grazing angle θ, or a combination of these quantities. NR can be

TABLE I. Neutron scattering length b of some elements and isotopes relevant to biological interfaces. Except for hydrogen where two isotopes are considered , these values represent the coherent scattering length for the mixture corresponding to the natural abundance of isotopes. Data taken from Ref. 7.

Element (or isotope*)	b (fm)
^{1}H*	−3.74
^{2}H (D)*	6.67
C	6.65
N	9.36
O	5.80
Na	3.63
Si	4.15
P	5.13
S	2.85
Cl	9.58

modeled by standard optical calculations using the relationship that the refractive index, for neutrons, of a material n is given by

$$n = 1 - \lambda^2 \frac{\sum_i b_i/V}{2\pi}, \tag{1}$$

where $\Sigma_i b_i$ is the sum of scattering lengths of elements in volume V. It is a conventional approach to construct appropriate multilayer models that assume a uniform refractive index in each of a series of layers parallel to the interface. The scattering lengths of all stable isotopes are available in literature. The interfacial excess of a species can be readily calculated from the fitted values of the scattering length density $\rho = \Sigma_i b_i / V$. Each layer used in the calculation is characterized by a thickness, a scattering length density, and possibly, an interfacial roughness. A reflection model of these stratified layers can then be interpreted in terms of the physical structure of the interface. Table I shows the scattering lengths of some elements, and Table II contains the scattering length densities of some common materials relevant to NR with the conversion to the neutron refractive index.

A recurring concept in this review is the neutron reflectivity profile, which is the variation in the neutron reflectivity R with respect to the momentum transfer q,

TABLE II. Neutron scattering length density ρ and neutron refractive index at a wavelength of 10 Å, n, of some common materials relevant to NR experiments of biological applications at interfaces.

Material	ρ (10^{-6} Å^{-2})	n (10 Å)
H_2O	−0.56	1.000 009
Air	0	1.000 000
Silicon	2.07	0.999 967
Fused Quartz, SiO_2	3.41	0.999 946
Sapphire, Al_2O_3	5.83	0.999 888
D_2O	6.35	0.999 899

$$q = \frac{4\pi \sin\theta}{\lambda}. \tag{2}$$

The terminology shown in Eq. (2) explains how the acquisition of NR measurements in "monochromatic mode" or "time-of-flight mode" is equivalent. Monochromatic mode involves scanning of the incident angle of a neutron beam through a range of values of θ at constant wavelength.[8] Time-of-flight mode involves the measurement of a polychromatic pulsed neutron beam that is analyzed for λ by determining the velocity of each neutron at a single angle. In practice, combinations of these different methods are frequently used.[9] The description of theory of reflection either in terms of optical models or scattering theory is described by, e.g., Lekner.[10] In practice, exact calculations using recursive matrix methods for multilayer structures—such as those described by Parratt,[11] Abèles,[12] and Born and Wolf[13]—are straightforward to apply for the majority of applications. These calculations are preferred in most cases to calculations using scattering theory that must allow for a strong interaction potential, and can involve problems associated with mathematics of inverse transforms.

There are several distinct advantages of NR over other experimental techniques that permit a range of unique investigations in the study of biological layers at liquid interfaces. First, as shown in Table I, there is a strong difference in the scattering properties of the hydrogen isotopes ^{1}H and ^{2}H. Thus chemically equivalent samples that contain regions of different isotopic contrasts can be prepared to locate the positions and orientations adopted by specific molecules or submolecular groups or, indeed, by the solvent molecules surrounding a solute.[14] Second, it is often possible to match the neutron scattering properties of the solvent with those of the incident medium so as to provide a reflection signal that depends only on the content of the interfacial layer. This approach can lead to an elegant direct measure of the surface excess of an adsorbed species.[15] Third, neutrons can penetrate many materials and so can be used to study "buried" layers such as those at solid/liquid interfaces.[16] This feature is a particular advantage, for example, in a study of model biological membranes.[17] Most single crystals, such as silicon, sapphire, or quartz, are transparent to neutrons and can be used to support a range of chemical species or model membranes for studies of adsorption and structure. Fourth, in comparison with x-rays, neutrons are relatively gentle to soft matter and therefore they are well-suited to the study of biological material,[18] such as proteins,[6,19–22] biomacromolecules,[23,24] and lipids[25–27] with minimal damage to the samples and negligible changes in the structure from heating.

Recent advances in the production of deuterated molecules have increased the potential for contrast matching in biological applications. For example, many phospholipids can now be readily obtained with deuterium labeling of the alkyl or acyl chains or indeed of specific regions in the head group.[28] Proteins and peptides often contrast strongly with deuterated lipids but can also sometimes be prepared with deuterium labels themselves. Most unlabeled biomolecules

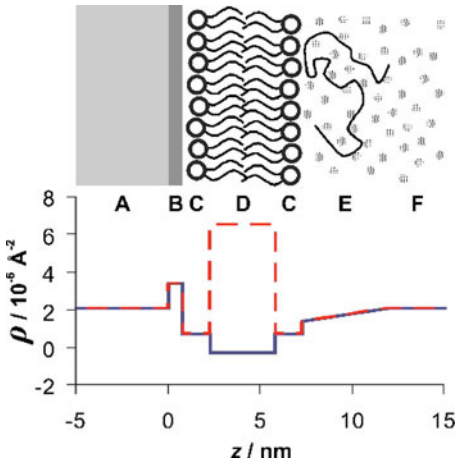

FIG. 1. A schematic of a model liquid/silica interface with a lipid bilayer and an adsorbed biopolymer. The lower panel shows profiles of the scattering length density ρ as a function of the distance z from the planar surface in the cases where the alkyl chain regions of the lipids are normal hydrogenous groups (continuous blue line) and deuterated groups (dashed red line). In both cases, the solvent is matched in scattering length density to that of the substrate. The different regions shown are (A) silicon, (B) silicon dioxide, (C) lipid head groups, (D) lipid alkyl chains, (E) adsorbed biopolymer, and (F) solvent.

such as proteins have a scattering length density that lies between those of H_2O and D_2O, but the precise value is likely to depend on the extent of exchange of H and D between the biomolecule and solvent. This use of isotopic labeling is illustrated by the schematic model of a biopolymer adsorbed to a lipid bilayer in Fig. 1, where the different scattering length density profiles of two chemically equivalent structures are shown. The value of deuterating the lipid chains is clear: the result is a marked enhancement of the scattering contrast with the biopolymer.

Enhancement of interfacial models by constraining them to fit multiple reflectivity profiles often removes the ambiguities associated with loss of phase information that are usual in scattering measurements, and thus can lead to unique information about surface composition. Inevitably, most biological interfaces comprise mixed species, so NR is particularly useful in quantifying the relationship between the bulk and surface composition. Additional useful features of NR result because the wavelength of neutrons is similar to that of molecular length scales, so uniform thin films can exhibit pronounced fringes, and repeating structures normal to the interface can generate Bragg diffraction peaks. Also, lateral inhomogeneity across the surface can appear as intensity in the off-specular scattering. Thus NR can help to reveal quantitative structural and compositional information about mixed systems, including phenomena such as adsorption, interfacial mixing, segregation, and displacement of one material by another.

There can be ambiguities in the interpretation of a reflectivity profile $R(q)$ in terms of the density profile $\rho(z)$ perpendicular to the surface, as different structural models may give rise to identical reflectivity. This drawback arises both from the loss of phase information about the wave in the scattering process mentioned previously and from the restriction that only a limited range of q is measurable. The major reason for the latter limit is that the reflectivity drops rapidly with increasing q (as q^{-4} for a sharp interface) and reaches the level of diffuse background scattering. In many cases, the ambiguity in structure can be resolved by providing additional information, such as a further reflectivity profile of the same biochemical environment but with known differences in the isotopic contrast. Prior knowledge of structural information, such as molecular composition or solution stoichiometry, can also be beneficial. The elucidation of complicated structures often relies on the use of multiple isotopic contrasts, which should ideally be chosen so as to provide clear information about different parts of the structure. For example, matching the neutron refractive index of all the components except one can be a useful means to determine the width of the distribution of that species.

A recent approach that can provide additional information without any physical change in the sample has been to include a magnetic layer as part of the substrate structure. This technique exploits the spin of the neutron, which can interact with a magnetic field so that two spin states will be reflected differently as though the magnetic layer in the sample has a different refractive index for the different directions of polarization. This methodology has been developed and exploited recently by Le Brun *et al.*[29] in a study of an antibody-binding membrane protein. Investigation of the binding of IgG with specifically created structures of protein on a substrate have been used in the development of novel sensors. This approach has the general advantage that two reflectivity profiles can be obtained from a single interface even for a sample that may be difficult to reproduce or prepare with different isotopic contrasts.

B. Analytical methods

Analysis of NR data to generate structural models of interfaces has advanced considerably in recent years. Most structural models are based on calculations of reflectivity using optical matrix methods based on the theory that is described above. This approach provides an efficient route to the simulation of reflectivity profiles for any given structure by dissection of the scattering length density profile normal to the interface into an appropriate number of stratified layers that are individually uniform in composition. In its simplest case, each layer is described by two parameters: a thickness and a scattering length density (or neutron refractive index). As an extension, a small roughness contribution can be included at each boundary using a simple procedure described by Nevot and Croce.[30] This roughness must be much smaller than the thickness of each adjacent layer. One of the most well-known and widely shared programs is an implementation of the algorithm of Parratt, which has been made available from the HMI Berlin.[31] Additionally, a number of programs that are available for free download, including Parratt, are cataloged by Rennie.[32]

The determination of a modeled scattering length density profile from a single reflectivity profile is not sufficient to

provide the structure of a multicomponent system. There are various approaches that enhance the interpretation of data. For example, one can constrain models to fit simultaneously multiple reflectivity profiles from the same biochemical environment recorded with different isotopic scattering contrasts of one or more components. If there is a known difference in scattering length density in spatial regions in multiple reflectivity profiles, possible ambiguity between different models that may give the same reflectivity is often removed. These types of constrained fits are easily extended so that if a layer consists of a mixture of two components, such as adsorbate and solvent, the scattering length density can be automatically calculated for the mixed layer when the solvent is changed. The program MOTOFIT (Ref. 33) is an example of this type of algorithm, which relates isotopic contrasts only and does not impose other constraints on a model. This functionality is now available in a number of other programs.

While traditional approaches have used least-squares minimization to optimize the fit of a model to data, the choice of starting parameters has often been important in finding a true minimum deviation. The choice of parameters and the variable to minimize (regularization) are important. While Marquardt algorithms are successful when parameters are close to a good fit, other algorithms such as "genetic" optimization are useful to explore a wider range of parameters, e.g., GenX as presented by Björck and Andersson.[34]

For complicated interfacial structures, there are often further constraints that can be imposed on layer structures in terms of the chemical composition, for example, of protein molecules or biopolymer chemistry. Building models with these constraints will often significantly reduce the number of free parameters in a fitting problem. In other cases, guidance from theory can be used to relate the composition and, hence, scattering length density of different layers. For example, just two or three parameters may be used to describe a smoothly varying profile for an adsorbed polymer rather than the individual thickness and density of many layers needed to calculate the reflectivity. Simple scaling theories for polymers have been included in programs such as CPROF (Ref. 35) but the approach can be taken much further (see Sec. I B 2, below).

Other constraints are also included in some software, such as defining layers in terms of the numbers of heads and tails of lipids or surfactants and the numbers of solvent molecules. It is much easier to verify that physically reasonable models are used and the fitting is much more stable in reaching a defined minimum if only a few parameters are required in the physical description of the system. A disadvantage of this approach to data analysis is that the resulting computer programs become less general in their application. Indeed, it may become necessary to use specifically tailored models for each type of experiment, which thankfully is not an undue burden with modern modular software. However, some programs for molecular monolayers and bilayers are available for general use and describe the structures in terms of heads, tails, and areas per molecule.[36]

Below we consider two alternative specific examples of NR modeling.

1. Multilayer model to fit Bragg diffraction peaks

Some reflectivity measurements are made on structures that consist of a pattern of multiple repeating layers. These layers will give rise to sharp peaks in the reflectivity profiles that are analogous to Bragg peaks in the diffraction from a crystal but in this case arise from one-dimensional order. Such structures can be observed after the adsorption of multiple layers of lamellar-phase phospholipids to a surface, in which case there is a repeating bilayer structure that is separated by an aqueous region. While it may be satisfactory in some cases to analyze these structures using simplified crystallographic software, for one-dimensional structures there are a number of special features that have lead to other approaches. Scattering theory, as applied in diffraction software, cannot model the reflectivity near the condition of total reflection, and the approach is often ill-suited to structures that are described in terms of average scattering lengths rather than specific atomic coordinates. However, the near surface lamellar structure of surfactants has been modeled using a calculation based on scattering theory by Penfold *et al.*[37] A simpler approach that uses the power of modern computers is simply to calculate the reflectivity using optical methods for a repeating structure. This has the advantage that the width of the Bragg peaks, which arise from a finite structure, is incorporated automatically in the calculation. This approach has been used recently in the study of organized structures that are found to form from the adsorption to solid surfaces of lipid-based nanoparticles.[25]

2. Lattice mean-field model to fit polymeric systems

A recent approach to simulate NR data of polymers on surfaces is worthy of discussion. The use of different polymer models to evaluate NR data is quite established as reported by Russell.[38] Polymer brushes, such as poly(*N*-isopropylacrylamide) (pNIPAAM), that are tethered to or grown on a solid support can undergo a triggerable phase transition. The trigger can be one or more of many stimuli, e.g., temperature, ionic strength, *p*H, light, electrical current, or protein adsorption. The design of stimulus-responsive functionalized polymers that undergo a phase transition around physiological temperature, *p*H, and ionic strength offers interesting potential in the field of novel drug delivery aids.

In the approach discussed here the different fitting parameters based on the specific polymer system itself were required, such as the internal state parameters (U_{AB} and g_{AB}) and Flory–Huggins interaction parameters ($\chi_{BB'}$) describing the copolymer-water interaction. In a proof-of-principle test, the parameters were determined independently of NR measurements using solubility data.[39] Molecular-based lattice mean-field theory, developed by Scheutjens and Fleer and Fleer *et al.*[40,41] for heterogeneous polymer systems as an extension of the Flory–Huggins theory,[42] was used. In order to model the responsive polymer brushes, the Scheutjens–Fleer

theory was extended with Karlström's polymer model,[43] as described by Linse and Björling.[44,45] This polymer theory is very general and is able to describe various phenomena such as self-association of polymers into various different morphologies, adsorption, and polymer-mediated forces between surfaces.[41]

The solution near the planar surface is divided into parallel layers. The thickness of the layers corresponds to the size of a polymer segment. Within each layer, a random-mixing approximation is applied and, hence, all lattice sites in a layer are equivalent. However, density gradients are allowed to develop perpendicular to the surface, and the equilibrium distribution of polymer is obtained by minimization of the free energy of the system.[44] Efficient numerical approaches[46] provide solutions typically within seconds on a simple computer, even though the theoretical description can be quite complex.

The polymer chains are assumed to be attached to a planar silica surface with the grafting density σ (the number of chains per lattice length squared). In addition to the solution interaction parameters, we need to assign values of (i) interaction parameters for the surface $\chi_{\text{surface},B}$, (ii) the degree of polymerization r_{polymer}, and (iii) the polymer grafting density σ. None of these values can be determined from direct measurements, but reasonable values of $\chi_{\text{surface},B}$ corresponding to a hydrophobic surface, $r_{\text{polymer}}=1000$, and $\sigma=0.08$ were used, of which σ was used as a fitting parameter to experimental NR data. A second fitting parameter is the factor d, which converts the lattice length unit into real length. It turned out that the predicted neutron reflectivity profiles were insensitive to the precise value of r_{polymer}, provided that the brush height remained the same by adjusting d. Thus, the fitting of the data for the polymer brush using the lattice polymer theory involved two parameters: σ and d. If the grafting density could be determined by an independent method, the number of fitted parameters representing the brush would be reduced to 1. All neutron reflectivity profiles were calculated from the structural models of the interface employing the standard optical matrix method.[2,11,12] Generally, the scattering length density of a layer ρ was evaluated according to

$$\rho = \sum_i \phi_i \rho_i + \left(1 - \sum \phi_i\right)\rho_{\text{solvent}}, \tag{3}$$

where ϕ_i is the volume fraction of component i in the layer, ρ_i is the scattering length density of component i, and ρ_{solvent} is the scattering length density of the solvent.

Figure 2(a) (solid curves) shows neutron reflectivity profiles predicted by the lattice mean-field polymer model; the dashed curves show fits carried out with a conventional layer model approach. Figure 2(b) shows the corresponding scattering length density profiles. Data are shown at two temperatures and in two solvent contrasts: D_2O and a mixture of H_2O and D_2O, which is contrast matched to the scattering length density of silicon [contrast matched silicon (cmSi)]. The value of d was first and uniquely determined by using the position of the fringes appearing in the cmSi data at the higher temperature [see the inset of Fig. 2(a)]. The value of σ was then adjusted to provide the best overall representation for the four conditions. It is clear that the lattice mean-field approach describes the experimental NR data better than the fit obtained by the conventional uniform layer model. In particular, a significant improvement is found for reflectivity data recorded in D_2O at $T=293$ K [Fig. 2(a)].

The lattice size length of $d=14.7$ Å obtained from the fitting compares well with the length of a few monomers and the grafting density $\sigma=0.08$, together with $d=14.7$ Å, imply a spacing of about 50 Å between the neighboring grafted polymers. The surface excess was 13 mg m^{-2} for the lattice model and 12 mg m^{-2} for the single layer model. This excellent agreement demonstrates that the novel fitting approach using lattice mean-field theory describes well the thermoresponsive polymer brushes. The new approach has several advantages. First, it requires only two fitting parameters, i.e., fewer than the six required with a constrained one layer model at two temperatures. Second, it captures self-consistently the thermal response of the polymer phase transition. Third, it provides a consistent description of the experimental data.

C. Complementary techniques

It can be particularly helpful in the study of interfacial problems with soft matter and biology to supplement NR measurements with data recorded using complementary techniques. Not only can precharacterization of biochemical systems before precious beam time reveal any practical problems with the preparation methods but also techniques with a smaller sampling size and faster kinetics can highlight inhomogeneity in the surface layer that should be considered in the analysis of the NR data. There are many relevant techniques including x-ray reflectivity, infrared reflection spectroscopy, and atomic force microscopy. In the discussion of the case studies in part II of the discussion, however, we refer to additional measurements using null ellipsometry, the quartz crystal microbalance with dissipation monitoring (QCM-D), and small-angle neutron scattering (SANS). Brief descriptions of the techniques and analysis are given here as a prelude to those discussions.

1. Null ellipsometry

Null ellipsometry is a technique that measures the change in polarization of elliptically polarized light upon its reflection at an interface.[47,48] The amplitude change (Ψ) and phase change (Δ) of the light upon reflection depend on the dielectric structure normal to the interface. One way to model the changes in Ψ and Δ is through carrying out a numerical fit to the refractive index n_x and thickness d of a single uniform layer. The validity of the calculated thickness breaks down for highly inhomogeneous layers but, as shown later, the values still provide insight into the layer formation. From the fitted values of n_x and d, the adsorbed amount Γ can be calculated using de Feijter's expression,[49]

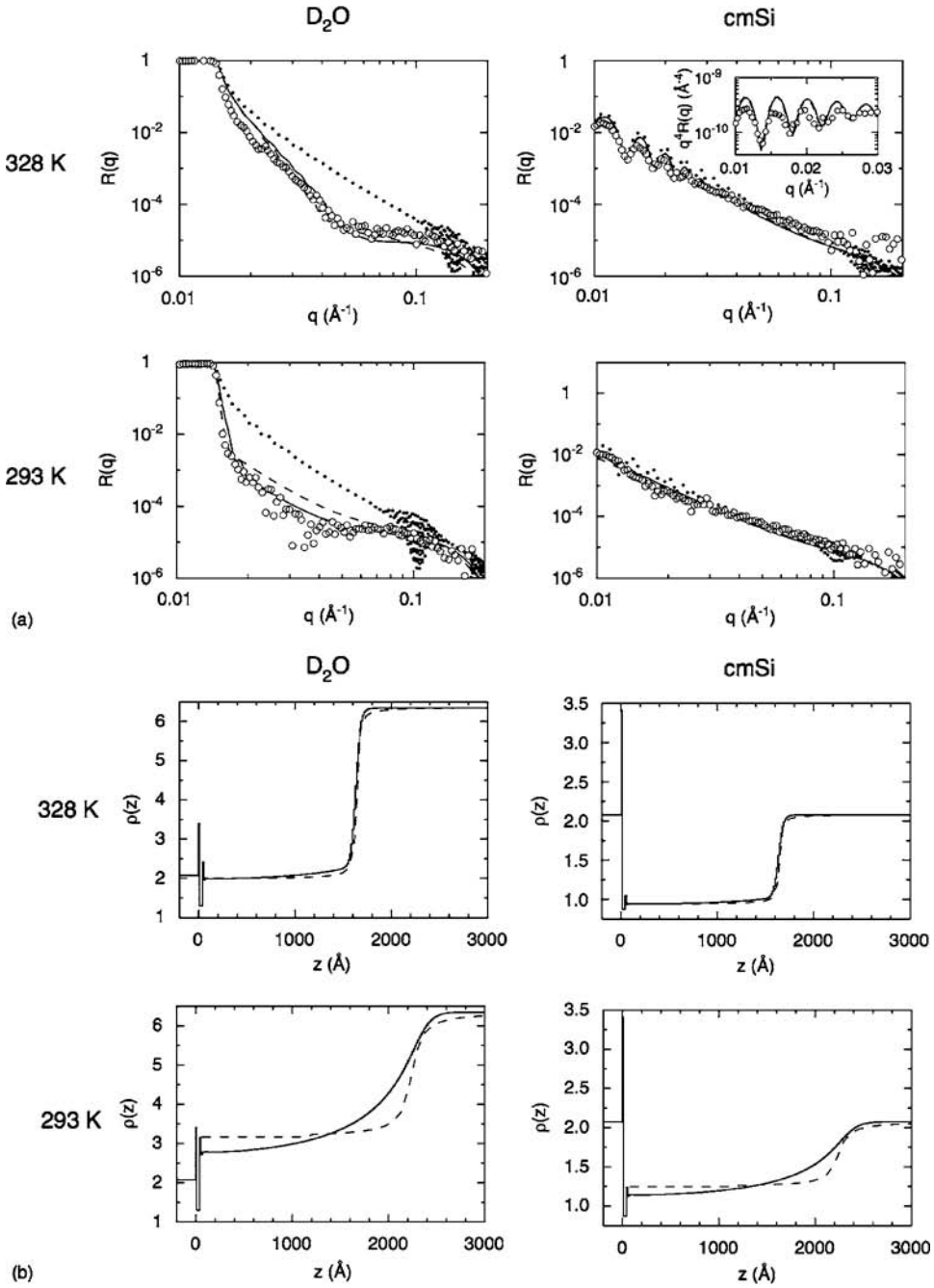

FIG. 2. (a) Experimental neutron reflectivity profiles (circles) and fitted profiles using a homogenous polymer layer model (dashed curves) and a lattice mean-field theory (solid curves) for polymers grafted on a Si/SiO_2/initiator surface at 328 K (top) and 293 K (bottom) in D_2O (left) and cmSi (right). Fitted neutron reflectivity profiles using a polymer layer model with zero roughness are also shown (dotted curves) to highlight the need for the inclusion of roughness in the fits. The top right panel contains an insert displaying clear fringes at low q in a plot of $q^4R(q)$ vs q. (b) Scattering length density profiles corresponding to the plots in (a). Data are taken from Zhang *et al.* (Ref. 39), where further details are given. (Reproduced by permission from the Royal Society of Chemistry.)

$$\Gamma = \frac{d(n_x - n_2)}{dn/dc}, \tag{4}$$

where dn/dc is the refractive index increment of the adsorbed layer and n_2 is the refractive index of the bulk solution.

2. Quartz crystal microbalance with dissipation monitoring

QCM-D is an acoustic technique where quartz crystals are resonated at multiples of their fundamental frequency through the application of alternating current across the crystal.[50,51] As molecules or particles adsorb to the surface,

the crystal mass increases and the resonance frequency decreases. However, it is important to remember that coupled water molecules also move with the crystal, so for viscoelastic films the decrease in frequency is a measure of the wet mass (Δm), and a simple linear (Sauerbrey) relationship with the increase in adsorbed amount is not valid. The dissipation factor (ΔD) is also measured when the applied current is stopped. Modeling of the changes in frequency and dissipation factor for nonrigid films leads to the viscoelastic properties of the adsorbed species and can reveal the structural features and provide insight into adsorption mechanisms.

3. Small-angle neutron scattering

SANS has developed into a powerful technique to study biomacromolecules and biomolecular complexes in solution.[18] The technique is applicable over a wide range of length scales ($\approx$10–1000 Å) and provides information about size, shape, domain orientations, conformational changes, and flexibility, as well as molecular assembly in solution. In a typical SANS experiment (after correction for detector response and calibration, and subtracting the background from the scattering intensity), the coherent differential scattering cross section $I(q)$ is obtained as a function of q and can be expressed as

$$I(q) = NV^2(\rho_s - \rho_p)^2 P(q) S(q), \quad (5)$$

where N is the number concentration of scattering entities, V is their volume, ρ_s and ρ_p are the scattering length density of the solvent and particles, respectively, $P(q)$ is a function known as the form or shape factor, and $S(q)$ is the interparticle structure factor. For a dilute system of noninteracting particles, the scattering only depends on $P(q)$, which can be derived theoretically for different shapes, such as a sphere or the core shell model.[52] As with NR, it is possible to tune the isotopic contrast so that selected parts of the scattering particle become invisible to the neutron beam.

II. DISCUSSION PART 1: RECENT ADVANCES IN THE SUBJECT AREA

A. Introduction to drug and gene delivery

The main challenges when designing delivery systems for sparingly water-soluble components in food and pharmaceuticals are to increase the solubility of the component and to prevent aggregation and crystallization. Other challenges are to protect the drug from degradation during storage until it reaches its targeted site in the body. Different types of liquid crystalline phases are attractive as they have large capacity to solubilize both hydrophobic and hydrophilic compounds. They can also be prepared to give intriguing nanostructures. Realization that lipid phases can be dispersed into mimics of biological particle structures was a breakthrough discovery. The simplest and most studied of such structures are the lamellar phase dispersions of vesicles and liposomes (in literature, the term "vesicle" most frequently refers to a unilamellar aggregate, whereas the term "liposome" refers to a multilamellar structure) discovered by Bangham and Home in the 1960s.[53] The major requirement for liposome formation is the occurrence of a multiphase region that comprises the lamellar liquid crystal coexisting with an aqueous phase. The use of liposomal dispersions based on phospholipids as delivery vehicles was tested on humans by Gregoriadis *et al.*[54] already in 1974, where the results pointed to the potential use of these types of drug delivery vehicles in cancer chemotherapy. The modern developments in nanotechnology have open up new routes for "intelligent design to treat complex disease," as discussed in the review by Couvreur and Vauthier.[55] One aim is to make these new type of nanosized drug delivery vehicles responsive to external stimuli such as changes in temperature or *p*H.[56] This development has also meant that the whole arsenal of experimental techniques resulting from the development of nanotechnology has been made available to the scientist who seeks to develop drug delivery systems.

Today, major components in drug delivery vehicles are either lipids or polymers, where also metal colloids can be incorporated to obtain specific properties. Even simple vesicle systems have been developed with the so-called Stealth liposome (Stealth® is a registered trademark of Liposome Technology, Inc., Menlo Park, CA). They included phospholipids substituted with poly(ethylene glycol) chains of molecular weight from 1000 to 5000 Da,[57,58] where hydrophilic chains sterically stabilize the particle and repel plasma proteins.[59] Also, the formation of disklike lamellar aggregates with potential as drug delivery vehicles has been reported to form from vesicle dispersions.[60] In analogy with liposomal dispersions, nonlamellar phase particles can be prepared by dispersion formation in a multiphase region comprising a type 2 ("water-in-oil") nonlamellar liquid crystal in coexistence with a dilute aqueous phase. Liquid crystalline nanoparticles of nonlamellar geometry were probably first observed in a light microscopy study of fat digestion in the late 1970s (Ref. 61) (note that only later was it realized that these aggregates had a bicontinuous cubic structure). When compared to liposome dispersions, nonlamellar liquid crystals can only be partially fractionated into particles that are small enough by using simple dilution of a given phase and subsequent dispersion. The cohesion forces within the aggregate are simple too strong to break up the structure into colloidal particles without dispersing agent. Larsson[62] and Buchheim and Larsson[63] reported the preparation of the first versions of partially stabilized fragmented nonlamellar, cubic phase particles, almost two decades ago by using dispersions of unsaturated monoacylglycerols. These micrometer-sized particles were dispersed by mechanical breakup in the presence of micellar solutions of bile salts or caseins. The action of these agents was explained in terms of a formation of a lamellar envelope on the surface of the cubic phase particle.[62,63] Later, it was discovered that amphiphilic block copolymers are very efficient for the stabilization of lipid-based nanoparticles plus the simultaneous preservation of the inner cubic phase structure of the particles.[64–67] Barauskas *et al.*[68] devised a method to prepare monodisperse cubic phase nanoparticles, and they found that it was possible to control

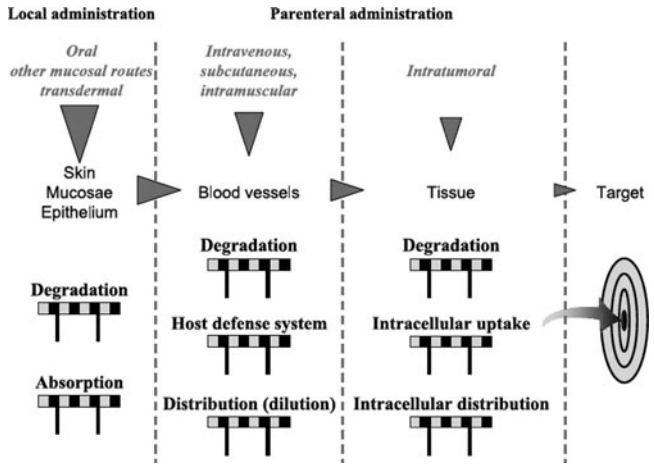

FIG. 3. A schematic drawing of the different hurdles, barriers, and interfaces that a drug delivery vehicle has to pass or interact with before the drug is delivered to its target. The loss of drug during its path to the target is illustrated by gray triangles. [With kind permission from Springer Science and Business Media, reproduced from Couvreur and Vauthier (Ref. 55), Fig. 2.]

further the dispersion particle size and nanostructure by varying the amphiphile concentration, the amount of charged species, and salt content. In fact, they showed that it is possible to prepare a range of different nanoparticle dispersions of self-assembled lipid mesophases with distinctive reversed cubic, hexagonal, and sponge phase structures by tuning the lipid composition using a simple, generally applicable and scalable method.[69]

There are many challenges when developing new drug delivery systems, as illustrated in Fig. 3, which shows the barriers and surfaces encountered along the different delivery routes before the drug meets the target. It is easy to understand that many different types of surfaces are encountered along this physiological route. It should also be noted that delivery is not only important in pharmaceutical applications but also in foodstuffs, as discussed in a recent book edited by Garti.[70] Today, considerable effort is based on *in vivo* and *in vitro* studies of the uptake of the drug, where focus is on drug release from the vehicle as well as transport and absorption of the drug.[71] Much less attention is directed to the process at interfaces, although there is considerable research activity in the biomaterials section.

There is vast literature on the delivery of biomolecules to interfaces, as cited above. In the following survey, we choose to focus on some important aspects that have been addressed with NR. The main focus is on the aspects of the use of lipids (or surfactants) as delivery vehicles, in addition to the main type of surface they encounter, namely, the biological membrane. We also address the behavior of DNA at interfaces and the effect of cationic surfactant, which is relevant to the transfer of DNA in the mammalian cells.[72] It is interesting to note that although a large number clinical studies of gene therapy is ongoing, only very few successful cures have been reported.[73] This research area still represents a huge challenge, where in particular the interfacial aspects are important.

B. Delivery of lipids and the formation of lipid bilayers: Recent advances with NR

There is an increasing demand for methods to study processes at the lipid/aqueous solution interface due to the importance of lipids and lipid self-assembly structures as regulators both for biological activity and for drug delivery vehicles. The biological membrane is one of the most important interfaces that the drug delivery vehicles encounter. The simplest proxy for the biological membrane in experimental studies is a phospholipid bilayer that can be prepared on a supporting solid surface in several different ways.[74–76] Spreading of vesicles on surfaces is an established method of forming bilayers on hydrophilic surface; spreading can be affected by the surface properties as well as properties that affect the stability of the vesicles. The spreading process itself is interesting and the mechanism and kinetics of the process are not fully understood. This process for the formation of 1,2-dimyristoyl-sn-glycero-3-phosphocholine (DMPC) bilayers on silica surfaces has been studied using NR by Gutberlet *et al.*[77] Unfortunately, the time resolution did allow the initial step of vesicle adhesion to be followed as with ellipsometry[78] and QCM-D.[79] However, the subsequent process, where the bilayer covered area grows with time, could be followed. They also tried to estimate the size of the lipid covered domains during the initial stage of the layer formation, by comparing two models to fit their NR data:

(1) Superimposing the reflectivity profile of the bare surface and that of the bilayer covered surface: *this model implies independent areas of phospholipid bilayer, which are larger than the coherence length of the neutron beam.*
(2) A phospholipid bilayer with a scattering length density between that of a complete bilayer and the solvent: *this model implies small defects in the bilayer (below the coherence length of the beam).*

Unfortunately, their data could be fitted equally well to both models.

Interesting questions are what happens if the vesicles consist of a mixture of lipids, and will one of the lipids be enriched next to the surface? These questions have been addressed by Wacklin and Thomas,[80] who investigated the bilayer formation from small sonicated unilamellar vesicles composed of a mixture of 1,2-dioleoyl-sn-glycero-3-phosphocholine (DOPC) and d_{63}-1,2-dipalmitoyl-sn-glycero-3-phosphocholine (deuterated DPPC) on silica. They found that the vesicle, which was adsorbed from above the chain melting transition, gave asymmetric bilayers for the mixed vesicles. The DPPC, which has a higher chain melting temperature, was enriched in the bilayer leaflet next to the silica surface. Their results point to the fact that one cannot assume that the composition of a supported bilayer is the same in the outer and inner leaflets.

Another way to prepare bilayers is to solubilize the lipid with a nonionic surfactant, e.g., DOPC in *n*-dodecyl-β-D-maltopyranoside (DDM). The bilayer formation is then

achieved by a series of subsequent additions of mixed lipid/surfactant solutions of decreasing total concentration, followed by a rinse after each step with acidic solution to remove the excess of the soluble surfactant.[26,81] This method is based on gradually approaching the two-phase region of the lipid/surfactant aqueous system, and thereby causing the deposition of a phospholipids bilayer. The issue here is how the lipid is transported from the mixed micelles to the surface or the incomplete bilayer. The process has been studied by NR where either the surfactant[26] or the lipid[25] has been deuterated. One hypothesis suggested by Vacklin *et al.*[26] based on their NR studies is that the mixed micelles diffuse within the stagnant layer and spread at the surface. This hypothesis was further supported by dissipation measurements using QCM-D, which can probe such extended structures at low surface coverage.[25]

One issue that arises from the work of Wacklin and Thomas[80] is the effect of the physical properties of the substrate on the quality of the bilayer. The influence is thought to be reduced by forming the bilayer on a polymer cushion.[82,83] Another advantage of the polymer cushion approach is that such a layer can provide a large aqueous cavity between the bilayer and the surface, which ensures that the bilayer is fully hydrated. These types of polymer-supported membranes have been discussed eloquently by Tanaka and Sackmann[84] in terms of models of the cell surface and the phenomena that occur at and across the interface including transport and peptide and protein binding. They also discussed different strategies to prepare these types of model cell membranes. One approach is simply to adsorb a polymer on a silica surface. This method has been investigated using NR by Wong *et al.*[82] They investigated different ways to form a DMPC bilayer on poly(ethylene imine)-coated quartz substrates. It was found to be important that the polymer film was dried before depositing the lipid, as otherwise no organized bilayer was formed and the swelling of the polymer layer was slower than the vesicle deposition rate. Once the bilayer was formed, it remained intact during the swelling of the polymer cushion, which when fully swollen had a polymer volume fraction of 0.15–0.20. It is interesting to note that polymer adsorption to a DMPC bilayer, formed by vesicle deposition, also gave a lipid bilayer sitting on a polymer-coated surface. This process is illustrated in Fig. 4. From the scattering length density profile, it is apparent that volume fraction of polymer in the space between the bilayer and the surface is quite low (~0.2). The cushion is also thinner (~40 Å) compared to when the bilayer is formed on top of the polymer layer (~180 Å when fully swollen). These results indicate that the poly(ethylene imine) is able to penetrate through the bilayer and adsorb to the quartz surface, which is a process driven by the strong electrostatic attraction between the polymer and substrate.

One problem with the bilayer being supported by a surface or floating on a polymer cushion is that the organized structure might be destroyed by shear forces or by an increase in the electrolyte concentration. This risk can be reduced by anchoring the lipid bilayer to the polymer

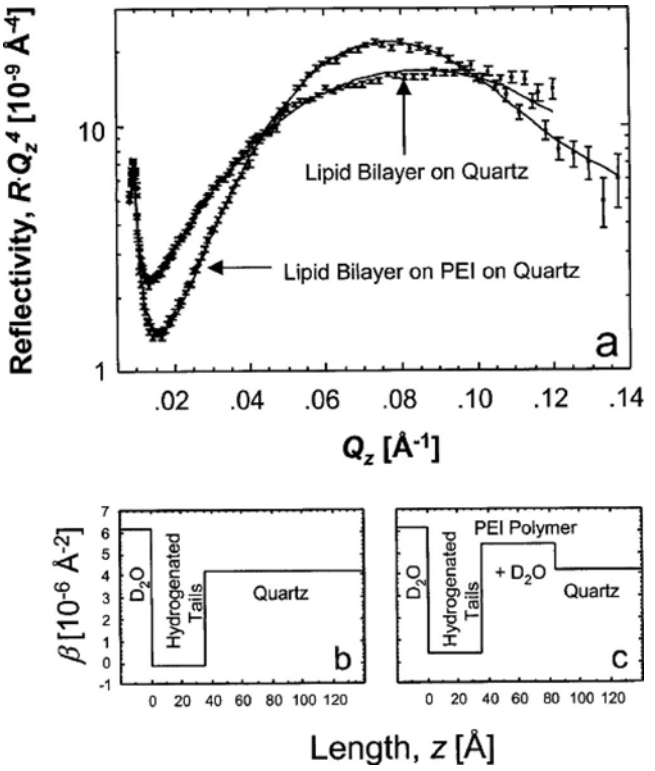

FIG. 4. (a) Neutron reflectivity profiles of DMPC bilayers formed by vesicle deposition on bare quartz substrates, where one layer was exposed to a cationic polymer, poly(ethylene imine) (PEI), which adsorbed from a 150 mM KNO_3 solution and penetrateds through the bilayer to form a polymer cushion. The corresponding scattering length density profiles are shown (b) without and (c) with exposure to the polymer. Figure is reproduced from Wong *et al.* (Ref. 82) with kind permission from the Biophysical Society.

cushion.[83,85,86] The general structure of an anchored bilayer is:[86] [surface linker]–[hydrophilic polymer tether]–[lipid backbone]–[lipid tail(s)]–[lipid monolayer]. The surface linker can be of chemical nature, e.g., a thiol compound that links to a gold surface[86] or polymer that adsorbs strongly onto the surface such as polylysine on silica.[83] The distance between the supporting substrate and the lipid layer is regulated by hydrophilic tethers,[86] but it is also possible to regulate the distance by the so-called layer-by-layer deposition,[83] i.e., sequential adsorption of oppositely charge polymers. The lipid backbone can be directly linked to the hydrophilic linker that, in turn, can be either covalently linked to the anchor[86] or can be a hydrophobically modified polyelectrolyte,[83] which has a charge opposite to that of the anchor polymer layer. The final lipid layer can then be deposited by the vesicle deposition, as discussed above, or by the rapid solvent exchange technique,[86,87] which basically means adsorbing the lipid from ethanol solution and then rapidly changing the solvent to buffer. NR is a useful technique to verify the structure of these layers, given their complex structure. The approach is arduous: it requires a substantial amount of modeling, systematic characterization during the build up of the layer, and use of complementary techniques such as x-ray reflectivity.[86] Phase sensitive NR makes it possible to, in principle, obtain a unique scattering length den-

sity profile without any knowledge about the composition of the layer. In practice, this approach requires that the multiple reflectivity profiles are acquired on chemically identical layers that were produced on different substrates, or that the layer is in contact with another sample environment that does not change its scattering length density profile. The former approach was used by Perez-Salas *et al.*[83] to characterize an anchored biomimetic polymer lipid bilayer, consisting of a polyelectrolyte multilayer plus synthetic terpolymer and a phospholipid layer. For this purpose, identical layers were prepared on silica and Al_2O_3, and reflectivity profiles were recorded on the two surfaces to obtain the phase information. They could determine the scattering length density profile of the layer with good accuracy.

An interesting approach to obtain a water cavity below a lipid bilayer is to carry out the deposition on a mesoporous substrate, as demonstrated by Doshi *et al.*[88] As verified by NR, a perfect bilayer with an estimated area per molecule of 44 ± 7 Å^2 (from the scattering length density of the layer) was formed by deposition of small unilamellar vesicles of 1-palmitoyl-2-oleoyl-sn-glycero-3-phosphocholine (POPC) on ordered nanocomposite and nanoporous silica thin films. The high bilayer coverage was suggested to be an effect of topography as well as the chemical properties of the nanoporous silica.

Another way to prepare bilayers that are "isolated" from the support is to prepare a stack of bilayers. This preparation can be achieved by using a chemically grafted phospholipid layer as the support for another bilayer floating on top, as described by Hughes *et al.*[89] They showed by NR that the hydration layer in the gel phase between the grafted bilayer and the top bilayer has a thickness of 17.5 Å. Furthermore, the grafted bilayer remained intact even when the top one was removed, which demonstrated the possibility of the removal of one bilayer only. NR has been used to determine the detailed organization and hydration of phospholipid bilayer stacks on surfaces, as shown by Haas *et al.*,[90] who also determined how myelin basic protein affects the multilayer structures.

There are many other NR studies on biomimetic lipid membranes, which have been recently summarized in the excellent review by Fragneto and Rheinstädter.[91] Many such studies include x-ray reflectometry as well as NR.[92,93]

For delivery of drugs, the interaction between the drug vehicle and lipid membrane is important. Furthermore, the interaction is particularly important for gene delivery systems where the vehicle needs to penetrate the membrane. This process can occur also with cationic polymers, as for poly(ethylene imine) penetrating the DMPC bilayer described earlier. Callow *et al.*[94] used NR to study the interaction of cationic lipid vesicles, of particular interest as gene delivery vehicle, with model cell membranes. The cationic vesicles comprised dimethyldioctadecylammonium bromide (DDAB) alone or with either 1,2-dioleoyl-sn-glycero-3-phosphatidylethanolamine (DOPE) or cholesterol. The lipid membrane was prepared by Langmuir–Blodgett (first layer) and Langmuir–Schaeffer (second layer) techniques on silica, using a 9:1 molar ratio of d_{63}-1,2-dimyristoyl-sn-glycero-3-phosphocholine (d-DMPC) and hydrogenated 1,2-dipalmitoyl-sn-glycero-3-[phospho-L-serine] (DPPS), and giving a negatively charged membrane. The pure DDAB vesicles were found to interact very weakly with the lipid bilayer and only after 15 days could some exchange of lipid be detected. No sign of forming an outer layer of DDAB was observed. This finding is somewhat surprising, as they observed that the DDAB vesicles interacted strongly with the bare silica surface. The reflectivity profiles for the interaction of DDAB/cholesterol vesicles with the model membrane show that the scattering length density of the lipid layer decreases with time [see Fig. 5(a)]. The change is much faster than for the pure DDAB vesicles. The fitted scattering length density profiles, shown in Fig. 5(b), suggest that there is an increase in the amount of hydrogenated material with time,

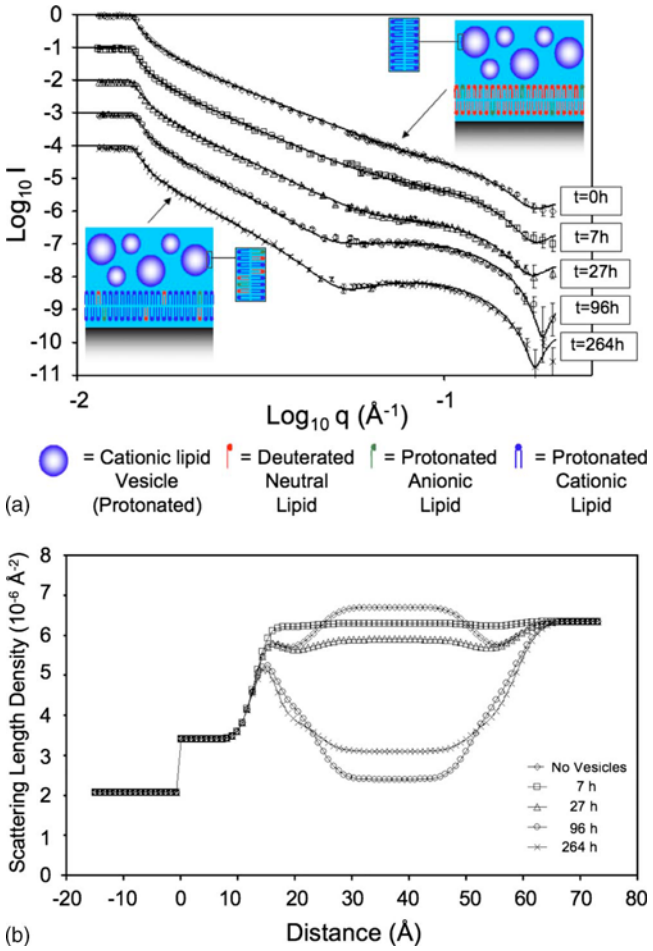

FIG. 5. (a) Neutron reflectivity profiles for a 9:1 *d*-DMPC:DPPS bilayer as a function of time after adding 0.1 mg/ml 1:1 DDAB:cholesterol vesicles, suspended in D_2O, as a function of time. The unexposed 9:1 *d*-DMPC:DPPS bilayer in D_2O (open diamonds), 7 h after exposure to DDAB:cholesterol vesicles (open squares), 27 h after exposure (open triangles), 96 h after exposure (circles), and 264 h after exposure (crosses). Solid lines represent model fits to the experimental data corresponding to the scattering length density profiles in (b). [Reprinted with permission from Callow *et al.* (Ref. 94). Copyright (2005) by the American Chemical Society.]

i.e., penetration of DDAB/cholesterol into the lipid bilayer. The extent of the change in the scattering length density can only be explained if there is an exchange so that some of the phospholipids leave the bilayer and are absorbed by the DDAB/cholesterol vesicles. Furthermore, it is noteworthy that the scattering length density profiles are consistent with that of a bilayer on the surface; no significant change in the thickness is observed due to the interaction with the vesicles. These results show that extensive vesicle adsorption does not take place. The DOPE-containing vesicles were found to interact faster with the membrane than those containing cholesterol. In this case, a significant amount of lipid exchange occurred. The larger effect of DOPE on the DDAB vesicle interaction can be explained possibly by the fact DOPE tends to form reversed liquid crystalline phases and, hence, destabilizes bilayer structure and possibly the fact that the DDAB facilitates the exchange between the vesicles and model lipid membrane.

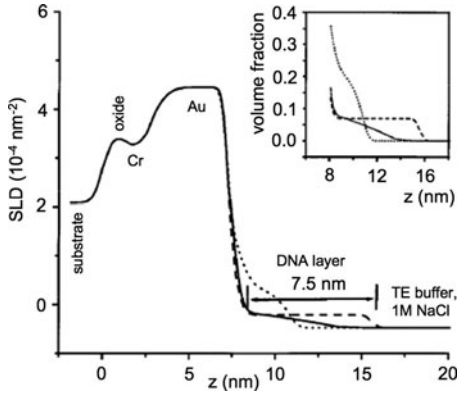

FIG. 6. Scattering length density (SLD) profiles determined from NR, showing the results for adsorbed HS-ss-DNA monolayer (dotted line), mixed HS-ss-DNA/MCH monolayer (solid line), and mixed HS-ss-DNA/MCH monolayer after hybridization (dashed line). Inset: corresponding DNA volume fraction profiles. [Reprinted with permission from Levicky *et al.* (Ref. 114). Copyright (1998) by the American Chemical Society.]

C. Delivery of DNA: Recent advances with NR

We are today fascinated by the supramolecular structures formed by DNA packing in the cell nucleus, and we are trying to understand as to what extent packing regulates transcription/translation.[95–97] The interactions between DNA and charged colloids[98–100] can be used as models for understanding the driving forces for DNA packing into cells.[101] Complexes of DNA and cationic macroions (lipid assemblies or polyelectrolytes) can potentially also be used as nonviral vectors for gene delivery.[102]

In order to deliver DNA systemically, such complexes must be designed to circulate in the blood stream for hours.[103] Under these conditions they will encounter different types of species in the bulk solution and at interfaces. These species are likely to interact and therefore influence the uptake of the DNA for the gene delivery application. Therefore it is essential to understand both the bulk and surface interactions of DNA with various physiological species. NR and SANS, both with isotopic contrast variation, offer a unique capability to determine the composition of complexes and aggregates formed with different types of interfaces and in the bulk solution.

Adsorption of double-stranded (ds-) DNA to various types of colloidal particles was first investigated over 40 years ago.[104] Both single-stranded (ss-) and ds-DNA adsorb onto hydrophobic substrates,[98,105–107] which is likely to be due to the entropic gain as water molecules that were confined at the hydrophobic surface are displaced into the bulk solution. In general, ss-DNA adsorbs to a greater extent than ds-DNA,[107] which is due to the larger exposure of the hydrophobic moieties in ss-DNA.[108] This has been demonstrated by SANS for polythymidylic acid (dT_{35}, M_w=13 416 g mol^{-1}) adsorption on aminated polystyrene latex particles, where the adsorption at high *p*H is still significant although the cationic charge is reduced.[109] Furthermore, the adsorption seems to be irreversible, that is, the DNA fragments stays on the particle even if the coated particles are subject to several rinsing steps. The dT_{35} was also found to adsorbed quite flat on the particle surface and only if the polynucleic acid is grafted with high density on the particle and if the *p*H is high (about 9) an increase the thickness of the layer is observed, i.e., the dT_{35} extends more from the surface.

The issue of orientation of DNA and its fragments is, of course, also interesting for bioanalytical applications, where the key property of functionalized particles and surfaces is their ability to hybridize with complementary DNA strands.[110–117] One of the key issues is the control of the nonspecific interaction of DNA with the surface. Here NR is a particularly useful tool, as demonstrated in the late 1990s

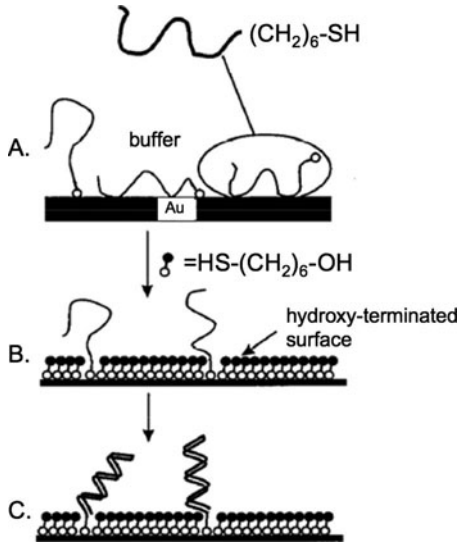

FIG. 7. (A) Functionalized single-stranded DNA (HS-ss-DNA) that adsorbs to the gold substrate through the thiol end group as well as through backbone-substrate contacts. A multitude of adsorption states exists. (B) The formation of a mercaptohexanol (MCH) monolayer that prevents contacts between the DNA backbone and the substrate, the HS-ss-DNA is left attached by the thiol end. (C) The end-tethered HS-ss-DNA is shown after hybridization to complementary oligonucleotides. [Reprinted with permission from Levicky *et al.* (Ref. 114). Copyright (1998) by the American Chemical Society.]

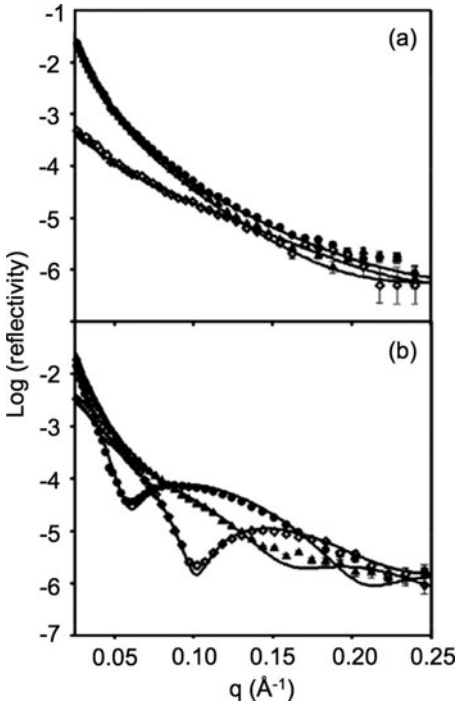

FIG. 8. Neutron reflectivity profiles for 300 base pair DNA (120 ppm) with C_{12}TABr concentrations of (a) $10^{-4}M$ and (b) $10^{-2}M$. Three different isotopic contrasts are used *d*-C_{12}TABr in NRW (null reflecting water with a scattering length density equal to zero; open diamonds), *d*-C_{12}TABr in D_2O (filled triangles), and C_{12}TABr in D_2O (filled circles). [Reprinted with permission from Zhang *et al.* (Ref. 121). Copyright (2008) by the American Chemical Society.]

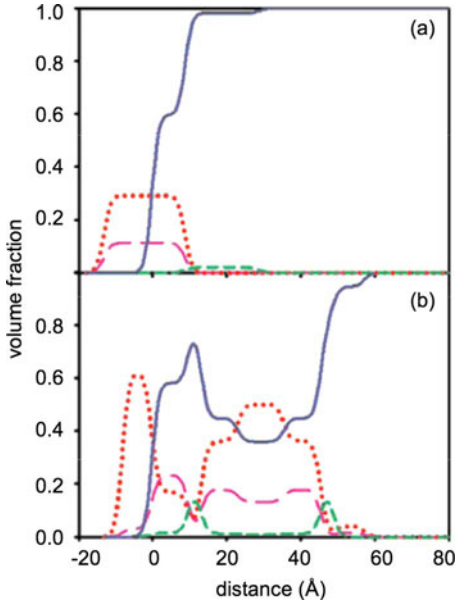

FIG. 9. The volume fraction profiles corresponding to the best fit to the neutron reflectivity profiles shown in Fig. 8 for 300 base pair DNA (120 ppm) with C_{12}TABr concentrations of (a) $10^{-4}M$ and (b) $10^{-2}M$. The layer used for the fitting corresponds to surfactant heads (pink long dashes), surfactant chains (red dots), DNA (green short dashes), and water (blue solid line). [Reprinted with permission from Zhang *et al.* (Ref. 121). Copyright (2008) by the American Chemical Society.]

by Levicky *et al.*[114] by determining the layer density profiles of oligomeric DNA monolayers on gold surfaces. They used ss-DNA that was functionalized at the 50 end with a thiol group (HS-ss-DNA). The concentration profiles determined from NR are reproduced in Fig. 6, and the main findings of their work are summarized schematically in Fig. 7. The adsorbed layers of HS-ss-DNA on bare gold are clearly compact, suggesting the presence of multiple contacts between each DNA strand and the surface, i.e., HS-ss-DNA interacts with the gold surface both via thiol-specific and nonspecific interactions. If the surface is treated with mercaptohexanol (MCH), which is a short alkanethiol with a terminal hydroxy group, then the grafted DNA molecules change their conformation and extend further into the solvent phase. These changes are consistent with the DNA remaining attached to the gold through its thiol end group, while contacts between DNA backbones and the surface are prevented by the formation of a mercaptohexanol monolayer. Last, the adsorbed HS-ss-DNA layer readily hybridized to its complementary sequence, which results in DNA helices with a preferred orientation toward the substrate normal.

It is well established that DNA, which can be regarded as a stiff extended anionic polyelectrolyte in aqueous solution, can be compacted by cationic surfactants, such as hexadecyltrimethylammonium bromide (C_{16}TABr), and the process is highly cooperative.[118,119] This phase behavior can be used to control the adsorption and structure of DNA at interfaces. If C_{16}TABr is added to a hydrophobized silica surface that has been precoated with DNA, the adsorbed amount increases while the layer thickness decreases.[107,120] The cooperative nature of the interaction between the cationic surfactant and DNA is also observed at the air/water interface, as reported by Zhang *et al.*,[121] who used NR to study the interaction between DNA and C_{12}TABr. They found that the surfactant was necessary to bring the DNA to the interface. The layer structure formed depended strongly on the length of the DNA, where the high molecular weight calf thymus DNA (50 000 base pairs, $M_w \approx 30\,800$ kDa) formed a thin layer with the surfactant of about 19–26 Å with only a minor effect of the C_{12}TABr. However, the low molecular weight salmon sperm DNA (300 base pairs, $M_w \approx 185$ kDa) underwent a distinct change from a monolayer structure to a much thicker layer at higher C_{12}TABr concentrations, as apparent from the appearance of a distinct diffraction peak at $q \approx 0.1$ Å^{-1}, indicating an overall layer thickness of about 60 Å. The layer structure was further analyzed in multiple isotopic solutions contrasts [null reflecting water (0.081 mol fraction of D_2O in H_2O) and D_2O], in combination with hydrogenous and deuterated surfactants (C_{12}TABr and *d*-C_{12}TABr). Some of the main results from the study of Zhang *et al.*[121] are given in Figs. 8 and 9, where the neutron reflectivity profile and the volume fraction profiles, respectively, are shown. The data at low surfactant concentrations ($10^{-4}M$) could be fitted to a monolayer of surfactant

(22–26 Å) with a rather thin layer of DNA, as apparent from the volume fraction profile in Fig. 9(a). As discussed in the paper, the DNA volume fraction in the layer is quite low and, therefore, the determination of the DNA layer thickness is not very accurate. This challenge is quite common when evaluating NR data for dilute layers of polymers. The data fits can be improved partly by optimizing the isotopic contrast and partly by the application of theoretical polymer models, as described in Sec. I. At higher surfactant concentration,[9,10] the layering is more distinct and fitting of the data suggests a surfactant monolayer next to the surface, then a thin DNA layer, then a C_{12}TABr bilayer, and lastly, a very dilute DNA layer. The overlap between the surfactant and DNA layers reflects that the C_{12}TABr layer is not very densely packed, which leads to the penetration of DNA into the surfactant head group region. Zhang *et al.*[121] explained the difference between the low and high molecular weight DNAs in terms of its rigid nature, where the short DNA is stiff and unable to wrap around surfactant micelles in solution; hence, it prefers to be located at the interfacial region, forming a layered structure.

The importance of charge density for the interaction between DNA and a cationic lipid at the air/water interface was investigated with NR by Wu *et al.*[122,123] They found that 700 base pair DNA interacted strongly with DC-cholesterol (3-β-[*N*-(*N*′,*N*″-dimethylethane)carbamoyl]-cholesterol) forming a densely packed 10–12 Å thick DNA layer, where the volume fraction of DNA is ~0.50, while the corresponding layer below the TC-cholesterol (3-β-[*N*-(*N*′,*N*′,*N*′-trimethylethane)carbamoyl]-cholesterol) contained 0.25 volume fraction DNA.[123] This discrepancy is likely to be due to a subtle difference in the charge density of the cationic species at the interfaces. Such differences can strongly effect the interaction between DNA and cationic surfactants, which has been demonstrated by Chen *et al.*,[124] who found that there is optimal spacer length of cationic gemini surfactants, i.e., an optimum charge density, which gives rise to a maximum interaction with DNA. Wu *et al.*[123] also found that the interaction between the zwitterionic DPPC and DNA is very weak, with almost no adsorption of DNA onto the DPPC monolayer, while the amount of adsorbed material increases with the DC-cholesterol content. Generosi *et al.*[125] studied the interaction of DNA (200–1000 base pair) in spin coated lipid layers, consisting of mixture of the cationic 1,2-dioleoyl-3-trimethylammonium-propane chloride (DOTAP) and the zwitterionic DOPC, by x-ray reflectometry and NR. They found that DNA encouraged a more structured multilayer stack. The NR data of nonhydrated layers suggested that the DNA is located within the head group region of the lipid rather than between the bilayers. Based on data from complementary techniques it was concluded that the DNA strands are located in the boundary between DOTAP-rich and DOPC-rich domains of the bilayers. This structure did not seem to change when the lipid stack was hydrated.

III. DISCUSSION PART 2: RELEVANT CASE STUDIES

A. Interactions of lipid-based cubic phase nanoparticles with model membranes (a drug delivery application)

The potential use of nonlamellar lipid structures[65,68,69,126,127] as delivery systems in pharmaceutical, food, and cosmetic applications has invoked a number of studies of the assembly and interactions of cubic phases of these materials. One such system is a colloidal dispersion of the cubic liquid crystalline phase of glycerol monooleate (GMO) with the trademark Cubosome®, which has a well-defined particle size and morphology.[68]

For the potential functionalization of these types of nanoparticles with drugs, it is crucial first to determine how they interact with and respond to the types of interface they will be exposed to when entering the physiological system. We will discuss some aspects of what happens when a liquid crystalline lipid nanoparticle encounters a lipid bilayer. Null ellipsometry and QCM-D provide kinetic information about the adsorption and triggerable release of the nanoparticles. Using contrast matching of the supported lipid bilayer, NR makes it possible to assess the exchange of material from one ordered lipid phase to another. Together the three techniques provide insight into the interaction mechanism.

From a practical application point of view, an important feature of liquid crystalline lipid nanoparticles is the physical and chemical stability for extended periods of time. Using appropriate compositions, the stability of these particles can be very good and extend to periods of months or years at room temperature.

One of the primary issues to be addressed when assessing liquid crystalline lipid nanoparticles as drug delivery vehicles is the nature of their interactions with biological membranes. The interfacial behavior of GMO-based bicontinuous cubic phase lipid nanoparticles at hydrophilic and hydrophobic surfaces has been studied previously using *in situ* null ellipsometry.[128] Depending on the surface properties and presence of electrolytes, different adsorption scenarios were discerned: at hydrophilic silica, thick surface layers of lipid nanoparticles are generated by particle adsorption from dispersions containing added electrolyte. Insight into the structures that are formed and mechanisms of adsorption can be gained from analysis of the time evolution of the adsorbed layer properties with techniques such as ellipsometry and QCM-D. The adsorbed amount at silica surfaces initially increases proportionally with time and then levels off to reach a saturation value of around 8–9 mg/m^{-2}, which is more than double that which would be expected for a complete lipid bilayer. Even though the adsorption layer was modeled using a single homogeneous layer, which indeed is an oversimplification if the nanoparticles adsorbed intact, a comparison of the adsorbed amount and thickness can reveal information about the layer formation. The layer thickness stabilizes quickly at a plateau value of about 40–50 nm, sometimes after a brief oscillation that may reflect transient structuring at the interface. The analysis suggests an adsorp-

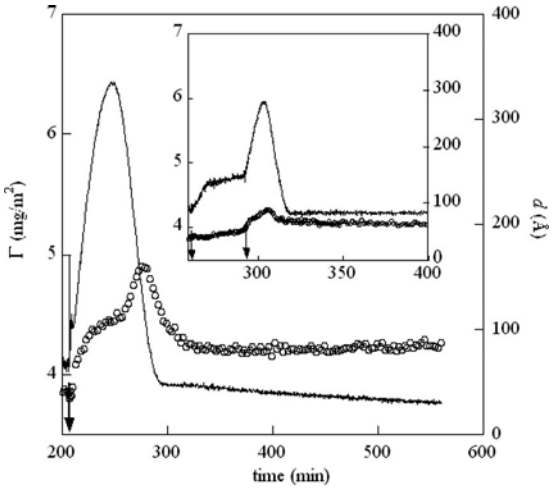

FIG. 10. Adsorbed amount Γ (line) and layer thickness d (open circles) determined by null ellipsometry as a function of time after the addition of cubic phase lipid nanoparticles at a concentration of 0.05 mg ml^{-1} on a DOPC bilayer at *p*H 4. The time of addition of the lipid nanoparticles is indicated by the arrow. The inset shows a sequential addition experiment with two different concentrations of lipid nanoparticles first at 0.001 mg ml^{-1} (indicated by the left arrow) then at 0.05 mg ml^{-1} (indicated by the right arrow). Data are taken from Vandoolaeghe *et al.* (Ref. 25), where further details are given. (Reproduced by permission from the Royal Society of Chemistry.)

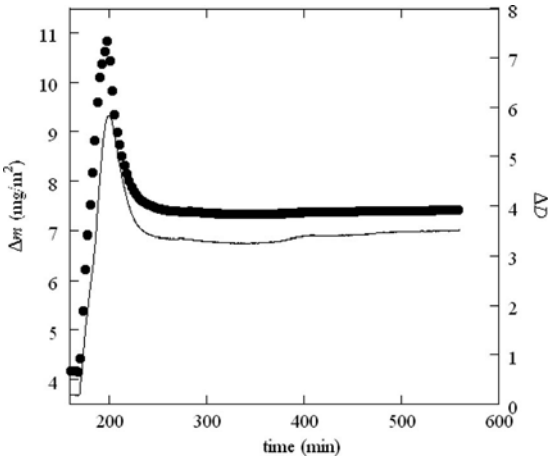

FIG. 11. Wet mass Δm (filled circles) and dissipation difference ΔD (line) determined by the quartz crystal microbalance with dissipation monitoring, obtained using a density of 1.050 g cm^{-3} from mass-uptake estimations using the Voigt-based viscoelastic modeling, as a function of time after the addition of lipid nanoparticles at a concentration of 0.05 mg ml^{-1} to a DOPC bilayer at *p*H 4. Note that the dissipation difference is frequency dependent and the values plotted here correspond to the third harmonic of the resonance frequency. Data are taken from Vandoolaeghe *et al.* (Ref. 25), where further details are given. (Reproduced by permission from the Royal Society of Chemistry.)

tion process where the interfacial layer is built up by attachment of an incomplete coverage of lipid nanoparticles rather than their molecular components. The adsorption at hydrophobically modified silica treated with an alkyl silane is dramatically different from that at bare silica. Adsorption is essentially independent of the presence of electrolyte or *p*H, and results in the formation of a thin, dense adsorbed layer, with a final thickness of 2–3 nm and an adsorbed amount of 1.7–2.0 mg m^{-2}. The analysis demonstrates that there is a formation of a monolayer and indicates that nanoparticles dissociate at this interface.

The interactions of these cubic phase lipid nanoparticles with surface supported model membranes of DOPC have been studied *in situ* using null ellipsometry, QCM-D, and NR.[25] In this work, the particles have a mean diameter of 170 nm, and three complementary techniques were applied to the problem to provide information about the mechanism of interaction.

Figure 10 shows the adsorbed amount and thickness of a modeled adsorption layer after the introduction of cubic phase lipid nanoparticles into the solution around a supported DOPC bilayer on silica.[25] The rapid increase in the adsorbed amount demonstrates that there is a strong positive interaction between the nanoparticles and the supported DOPC bilayer. As in the case of the bare surface interactions, the thickness increases beyond that of a single lipid bilayer, which is consistent with an incomplete coverage of nanoparticles. The adsorbed amount decreases after about 1 h, which shows that there is a net release of material from the surface. However, if a much lower amount of nanoparticles is first introduced into the system (first arrow in the inset), then there is no net release of material from the surface until the higher amount of nanoparticles is added (second arrow in the inset). These data show that the release of material from the surface can be triggered by the solution concentration of nanoparticles. Furthermore, this behavior suggests that instability of the fused particles may result after there is sufficient exchange of material. Unfortunately, ellipsometry does not have the capability to resolve conclusively the structure or composition of the lost material, and so two other surface-sensitive techniques were applied to the problem to provide further information about the interaction mechanism.

Figure 11 shows the changes in Δm and ΔD of an analogous experiment concerning the interaction of cubic phase lipid nanoparticles with a supported DOPC bilayer using QCM-D. Both these acoustic data and the optical data recorded with null ellipsometry reveal similar qualitative interfacial behavior: there are temporal maxima after 1 h in the adsorbed amount (null ellipsometry), wet mass (QCM-D), and change in dissipation (QCM-D). Through viscoelastic modeling of the surface layer, it can be shown that the wet mass comprises two-thirds water at a time corresponding to the maximum in the adsorbed amount, which is the reason for the difference in mass determined by ellipsometry and QCM-D. This high fluidity of the surface layer is not consistent with the interaction of the tiny amount of monomeric GMO in solution with the lipid bilayer, and so provides evidence that cubic phase lipid nanoparticles themselves adsorb intact during the initial interaction. Even so, the interaction mechanism on a molecular level had not been revealed by these two techniques, so NR was also applied to the problem.

Figure 12 shows neutron reflectivity profiles and fits in solution contrasts of D_2O for the interaction of lipid nanoparticles with a DOPC bilayer. Table III lists the fitted parameters. By using hydrogenated nanoparticles and a deuter-

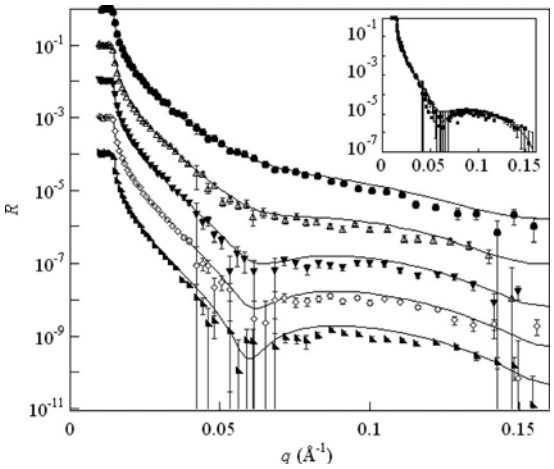

FIG. 12. Neutron reflectivity profiles (data) and fitting curves (lines) recorded after the addition of at a final concentration of 0.001 mg ml^{-1}, after (i) 0 min (*d*-DOPC bilayer) (filled circles), (ii) 15 min (open triangles), (iii) 90 min (filled inverse triangles), (iv) 165 min (open diamonds), and (v) 240 min (filled triangles) at *p*H 4. For clarity, the profiles have been displaced by a factor of 10. The inset is the reflectivity profile after 240 min with a fitting curve corresponding to the same fitting parameters but with a thick hydrogenated layer (2000 Å) on top and very high water content (93%). This model fit demonstrates that a low coverage of intact nanoparticles has a negligible effect on the reflectivity profiles, and hence the data from the NR experiment are consistent with some residual nanoparticles remaining attached at the interface after several hours. Data are taken from Vandoolaeghe *et al.*(Ref. 25), where further details are given. (Reproduced by permission from the Royal Society of Chemistry.)

ated DOPC bilayer in different solution contrasts, information was accessed about the composition of the interface as well as structural changes in the surface layer. A three-layer adsorption model (head groups, acyl chains then head groups) normal to the silica surface is sufficient to fit the data. A continuous decrease in the scattering length density and thickness of the acyl chain region is observed with time. At the end stage, the adsorbed layer is composed of an acyl chain region with a very low scattering length density, which is indicative of significant exchange having taken place between the nanoparticles (initially comprised hydrogenated GMO) and the deuterated DOPC bilayer. It follows that this exchange of material results in an instability of the fused particles, which is consistent with the observed net release of material from the surface with null ellipsometry. Here we note that the limited time resolution of the NR measurements would not allow the capture of the maxima in adsorption observed with ellipsometry and QCM-D.

To summarize, three surface-sensitive techniques have been used together to understand the mechanism of interactions between cubic phase lipid nanoparticles and supported lipid bilayers.[25] There is a rapid adsorption of intact particles onto the surface, followed by exchange of lipid material, which results in a net release of particles depending on the solution conditions. This interesting and controllable interaction of the nanoparticles with model membranes suggests that they do have potential in their intended use as a drug delivery aid. In this work, null ellipsometry revealed the adsorption kinetics, QCM-D revealed the interfacial structure,

TABLE III. Neutron reflectivity fitting parameters for a deuterated DOPC bilayer (0 min) and mixed adsorption layers at five different times (15–315 min) after the interaction of 0.001 mg ml^{-1} lipid nanoparticles: subscripts hg and ac stand for head group and acyl chain regions, respectively. For each layer fit, the solvent volume fraction (55% for the head groups and 45% for the acyl chains) and roughness (3 Å for the head groups and 8 Å for the acyl chains) were kept the same as for the bilayer.

Time (min)	d_{hg} (Å)	d_{ac} (Å)	ρ_{hg} (10^{-6} Å^{-2})	ρ_{ac} (10^{-6} Å^{-2})
0	7 ± 1	29 ± 3	1.8 ± 0.2	6.0 ± 0.3
15	7 ± 1	27 ± 2	1.8 ± 0.2	5.0 ± 0.2
90	7 ± 1	25 ± 2	1.8 ± 0.2	4.4 ± 0.2
165	7 ± 1	25 ± 2	1.8 ± 0.2	3.8 ± 0.2
240	7 ± 1	25 ± 2	1.8 ± 0.2	3.4 ± 0.3
315	7 ± 1	25 ± 2	1.8 ± 0.2	3.4 ± 0.3

and NR revealed the composition. Together the use of the complementary techniques has allowed us to construct a picture of the interaction mechanism with more certainty than could be achieved with any two techniques in isolation.

B. DNA compaction at surfaces and in the bulk solution (a gene delivery application)

SANS has been used to reveal the structure and composition of DNA-C_{16}TABr layers on various particles. The aims were realized through the use of deuterated polystyrene latex particles and a solvent that was contrast matched to the scattering length density of the particles, so that the neutron-scattered intensity recorded comes only from the adsorbed layer. The structure of the DNA layer on the particles was revealed.

Figure 13(a) gives the SANS data for DNA-coated particles with increasing concentration of deuterated C_{16}TABr.[24] Here the scattered intensity of neutrons that is recorded arises only from the DNA adsorbed layer since both the core of the particles and the cationic surfactant molecules are invisible to the neutrons. As the concentration of C_{16}TABr increased, the total scattered intensity decreases which is consistent with a lower proportion of DNA in the adsorbed surface layer. Moreover, the oscillations shift to larger q and eventually disappear for 1 mM C_{16}TABr. These observations point to a reduction in the total size of the coated particles as cationic surfactant is added, which is in agreement with DLS and null ellipsometry results.

Figure 13(b) gives the SANS data for DNA and hydrogenated C_{16}TABr. In this case, both the DNA and the C_{16}TABr are visible to the neutrons. Similarly, the total intensity progressively decreases, and the oscillations shift to larger q as the C_{16}TABr concentration is increased. The data were fitted to a core-and-shell form factor, confirming the decrease in the size of the shell upon addition of cationic surfactant. Additionally, C_{16}TABr was found to be evenly distributed within the adsorbed layer for the lowest cationic surfactant concentration used (where there was a large excess of negative to positive charges in the system, $\rho_{-/+}=36$). However, a core-and-shell model could not be used to fit the data

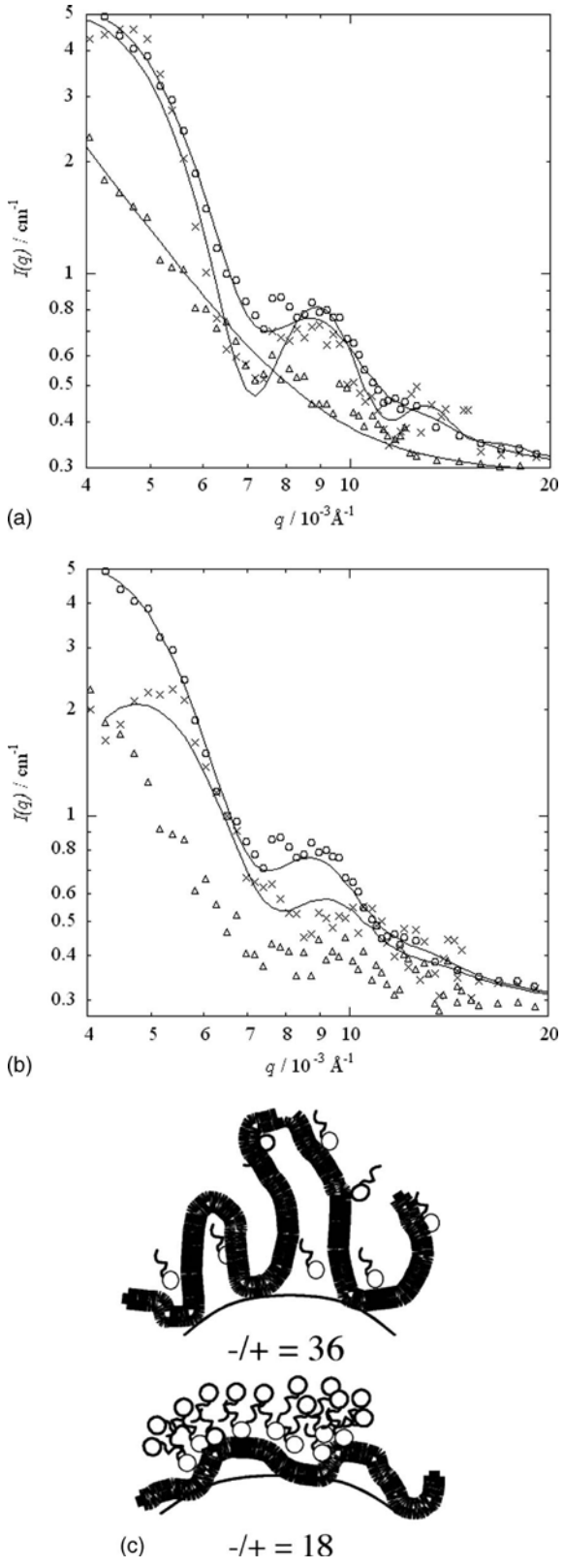

FIG. 13. SANS data for DNA in a 1% v/v dispersion of deuterated polystyrene–latex particles (circles) with (a) deuterated C_{16}TABr and (b) hydrogenated C_{16}TABr coated particles at bulk concentrations of 0.5 mM (crosses) and 1 mM (triangles). (c) A proposed structure for the DNA-C_{16}TAB coated particles. [Reprinted with permission from Cárdenas *et al.* (Ref. 24), where further details are given. Copyright (2005) by the American Chemical Society.]

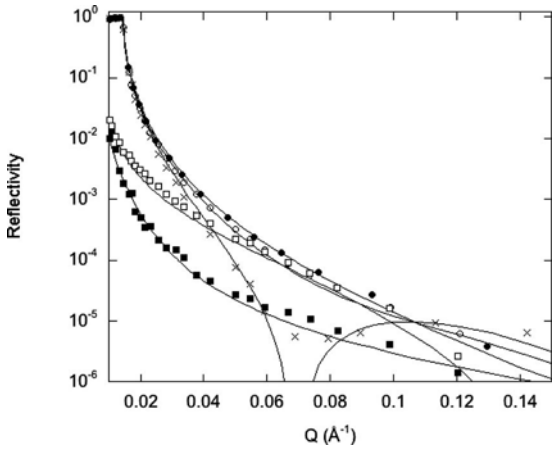

FIG. 14. Neutron reflectivity profiles for bare silica surfaces in D_2O (filled circles) and cmSi (filled squares), and DNA-C_{12}TABr adsorbed mixed layers for hydrogenated surfactant in D_2O (crosses) and deuterated surfactant in D_2O (open circles) and deuterated surfactant in cmSi (open squares). The curves represent the best fits to the data using a model of uniform layers. [Reprinted with kind permission from the publisher (Ref. 23, Fig. 9). Data are taken from Cárdenas *et al.* (Ref. 23), where further details are given.]

for DNA-coated particles containing 1 mM hydrogenated C_{16}TABr due to the development of a shoulder in the scattering profile at $q \approx 0.008$ A^{-1}. The position of this shoulder coincides with a shoulder observed in the absence of particles at similar conditions. Therefore large cationic surfactant aggregates, similar to those identified in the absence of particles, are also formed within the adsorbed layers where the excess of negative to positive charges in the system was reduced to $\rho_{-/+}=18$. At this charge ratio, the adsorbed layer decreased from 24 (for surfactant-free DNA coated particles) to 6 nm. The q values for the shoulder in the scattering profile imply an aggregate size of about 800 Å, and these dimensions, considering the type of aggregate the surfactant might form, suggest a rodlike micellar structure.

Figure 13(c) gives a schematic representation of the proposed structure for the adsorbed layers. Note that DNA compaction by cationic surfactant is more effective at surfaces than in the bulk solution: under similar conditions ($r_{-/+}=18$), there is only a 20% size reduction for DNA-C_{16}TABr complexes in the bulk compared with a 75 times reduction in the adsorbed layer thickness of coated latex particles. This discrepancy is a clear indication that formation of complexes between DNA and C_{16}TABr is facilitated by the surface.

DNA does not adsorb at similarly charged surfaces in conditions of low ionic strength (10 mM NaBr) due to electro-

TABLE IV. Values of the thickness and solvent content used in fits of a three-layer adsorption model (surfactant/DNA/surfactant) to the NR data in Fig. 8 [from Cárdenas *et al.* (Ref. 23)].

Layers	Thickness (Å)	Solvent content (vol %)
Inner surfactant layer	29	53
DNA layer	20	90
Outer surfactant layer	26	94

static repulsion. As C_{16}TABr is added to a DNA solution, the net negative charge of the complexes is decreased until eventually phase separation occurs, even before any adsorption occurs on the hydrophilic surface. However, for complexes of DNA with a lower molecular mass cationic surfactant, dodecyltrimethylammonium bromide (C_{12}TABr), a very slow adsorption process takes place at a DNA-C_{12}TABr molar charge ratio ($\rho_{-/+}$) of 0.3, which is just below phase separation.[129]

Complexes of DNA-C_{12}TABr form a ~50 Å thick monolayer onto negatively charged silica surfaces at charge ratios close to phase separation.[129] NR can give a more detailed picture of such layers. Figure 14 shows the neutron reflectivity profile for an adsorbed layer of DNA-C_{12}TABr complexes using three different contrasts: (i) hydrogenated C_{12}TABr in D_2O, (ii) deuterated C_{12}TABr in D_2O, and (iii) deuterated C_{12}TABr in cmSi.[23] The neutron reflectivity profiles contain information from both DNA and C_{12}TABr within the adsorbed layer for case (i), only DNA for case (ii), and mainly the C_{12}TABr for case (iii). The symbols in Fig. 14 represent the measured data, and the neutron reflectivity profiles correspond to the best fit with parameters given in Table IV (a self-consistent fit was used for the three data sets). It is obvious from the fits that the adsorption mechanism involves the formation of cationic surfactant admicelles on the surface that occupy a volume fraction of about half. On top of these admicelles, a low volume fraction layer ($<10\%$) of DNA is formed that is decorated by more surfactant molecules (the model that gives the best fit assumes a third layer composed of cationic surfactant). Thus DNA is not in direct contact with the surfaces but instead sits on a surfactant cushion. Interestingly, at the corresponding total concentration of free surfactant (assuming electroneutrality in the DNA-C_{12}TABr complexes), no significant C_{12}TABr adsorption from a pure surfactant solution is observed (null ellipsometry gives an adsorbed amount smaller than 0.05 mg m^{-2}). Therefore the presence of DNA in solution induces the adsorption of the surfactant.

What then is the driving force for the adsorption of DNA-cationic surfactant complexes to hydrophilic surface? Additional surfactant binding does not occur above a surfactant concentration slightly below the charge neutralization condition.[130] Consequently, an excess of free cationic surfactant is present in solution at a charge ratio between the total number of DNA (–) and cationic surfactant charges (+) $\rho_{-/+}=0.3$. It should be noted that no significant C_{12}TABr adsorption from pure surfactant solution is observed ($\Gamma < 0.05$ mg m^{-2}) at this low C_{12}TABr concentration ($6 \times 10^{-4} M$). Therefore we conclude that adsorption only occurs when the charge density of the DNA-C_{12}TABr complex approaches neutrality and the system is close to the expected phase separation limit. This phenomenon can be interpreted as a decrease in the solvent quantity for the DNA-C_{12}TABr mixtures.

For C_{16}TABr, phase separation occurs at a value of $\rho_{-/+} \approx 9$ without any adsorption at the hydrophilic surface. Indeed, the DNA-C_{16}TABr complexes are more stable in the bulk than those formed with C_{12}TABr.[131] Therefore the interactions between DNA and C_{16}TABr in the bulk solution are stronger than the interactions with the surface, and consequently, no adsorption takes place. Interestingly, the molecular weight and conformation (single- versus double-stranded chains) does not seem to influence the interfacial behavior of the mixed DNA-C_{12}TABr system at negatively charged surfaces. This observation supports the idea that it is the interaction with the surfactant that determines the adsorption process.

IV. CONCLUDING REMARKS

NR offers several significant differences compared with optical techniques such as ellipsometry or resonance spectroscopies in its capability to probe soft matter and biology at interfaces. Although deuterium and hydrogen scatter light similarly, they scatter neutrons very differently so that different isotopic contrasts can be achieved through selective deuteration of adsorbed molecules (or parts thereof) and the liquid subphase. Multiple neutron reflectivity profiles obtained for the same biochemical environment increases the reliability of the resulting characterization by removing ambiguity in the model fits of data. Quantitative structural and compositional information can all be determined from NR experiments. Also, details can be revealed about the internal structure of interfacial layers due to interference patterns because neutron wavelengths are of a similar order to molecular length scales.

In this review we have discussed how NR can be used to acquire knowledge of drug and gene delivery systems, where the crucial step in many cases is the interaction between the delivery vehicle and interfaces, such as catheters, vials, and last but not least biological membranes. NR has been a crucial technique for characterizing newly developed biomimetic membranes. We have also shown that complementary information, both modeling and the use of other experimental techniques can help in obtaining the most information from NR data.

Given the current expansion of this research area, many further applications will emerge in the future. The aim to determine quantitative information about the behavior of biomolecules at interfaces on the nanometer scale can in many cases be realized only by NR experiments, as they can readily distinguish different components in complex mixtures. Current developments will advance the characterization of biomolecules at interfaces in several distinct ways, such as investigation of in-plane, lateral structure using off-specular scattering from interfacial layers as a routine method. Important aspects are also the possibility to use smaller samples as well as facilities to provide selectively isotope, e.g., deuterium, labeling of biological compounds. Advances in sources and instrumentation offer the prospect of investigation of smaller samples or more rapid kinetic processes.

ACKNOWLEDGMENTS

The work in the two case studies involved quite a number of scientists from all over the world and we very much appreciate their contributions. Here we acknowledge in particular Robert K. Thomas, Fredrik Tiberg, Fredrik Höök, Cecile A. Dreiss, Chau P. Chan, Terence Cosgrove, Björn Lindman, Stefan Zauscher, Jianming Zhang, and Hanna Vacklin for their contributions and stimulating discussions. The authors are grateful for allocations of beam time at NIST Centre for Neutron Research, Gaithersburg, USA (NCNR) and Institut Laue-Langevin, Grenoble, France (ILL). We thank Sushil Satija for help with experiments at NCNR and Giovanna Fragneto and Roland May for help with experiments at ILL. Financial support from the Swedish Foundation for Strategic Research (SSF), the Swedish Research Council (VR), and the European Commission is much appreciated.

[1]J. Penfold and R. K. Thomas, J. Phys.: Condens. Matter **2**, 1369 (1990).
[2]J. Penfold, Curr. Opin. Colloid Interface Sci. **7**, 139 (2002).
[3]J. E. Bradley, E. M. Lee, R. K. Thomas, A. J. Willatt, J. Penfold, R. C. Ward, D. P. Gregory, and W. Waschkowski, Langmuir **4**, 821 (1988).
[4]T. L. Crowley, E. M. Lee, E. A. Simister, and R. K. Thomas, Physica B (Amsterdam) **173**, 143 (1991).
[5]J. R. Lu, T. J. Su, R. K. Thomas, J. Penfold, and R. W. Richards, Polymer **37**, 109 (1996).
[6]H. Xu, S. Perumal, X. Zhao, N. Du, X.-Y. Liu, Z. Jia, and J. R. Lu, Biophys. J. **94**, 4405 (2008).
[7]V. F. Sears, Neutron News **3**, 29 (1992).
[8]C. F. Majkrzak, S. K. Satija, N. F. Berk, S. K. Krueger, J. A. Borchers, J. A. Dura, R. Ivkov, and K. O'Donovan, Neutron News **12**, 25 (2001).
[9]R. Cubitt and G. Fragneto, Appl. Phys. A: Mater. Sci. Process. **74**, S329 (2002).
[10]J. Lekner, *Theory of Reflection of Electromagnetic and Particle Waves* (Martinus Nijhoff, Dordrecht, 1987).
[11]L. G. Parratt, Phys. Rev. **95**, 359 (1954).
[12]F. Abelès, Ann. Phys. (Paris) **5**, 596 (1950).
[13]M. Born and E. Wolf, *Prinicples of Optics*, 6th ed. (Cambridge University Press, Cambridge, England, 1980).
[14]D. J. Lyttle, J. R. Lu, T. J. Su, R. K. Thomas, and J. Penfold, Langmuir **11**, 1001 (1995).
[15]J. R. Lu, R. K. Thomas, and J. Penfold, Adv. Colloid Interface Sci. **84**, 143 (2000).
[16]G. Fragneto, J. R. Lu, D. C. McDermott, R. K. Thomas, A. R. Rennie, P. D. Gallagher, and S. K. Satija, Langmuir **12**, 477 (1996).
[17]S. Krueger, J. F. Ankner, S. K. Satija, C. F. Majkrzak, D. Gurley, and M. Colombini, Langmuir **11**, 3218 (1995).
[18]*Neutron Scattering in Biology*, edited by J. Fitter, T. Gutberlet, and J. Katsaras (Springer, Berlin, 2006).
[19]R. K. Thomas, Annu. Rev. Phys. Chem. **55**, 391 (2004).
[20]T. Nylander, F. Tiberg, T. S. Su, J. R. Lu, and R. K. Thomas, Biomacromolecules **2**, 278 (2001).
[21]J. R. Lu, Annu. Rep. Prog. Chem., Sect. C: Phys. Chem. **95**, 3 (1999).
[22]M. Cárdenas, T. Arnebrant, A. Rennie, G. Fragneto, R. K. Thomas, and L. Lindh, Biomacromolecules **8**, 65 (2007).
[23]M. Cárdenas and T. Nylander, in *Interaction of DNA with Surfactants and Polymers*, edited by B. Lindman and R. Dias (Wiley, Oxford, 2008), pp. 291–316.
[24]M. Cárdenas, C. A. Dreiss, T. Nylander, C. P. Chan, T. Cosgrove, and B. Lindman, Langmuir **21**, 3578 (2005).
[25]P. Vandoolaeghe, A. R. Rennie, R. A. Campbell, R. K. Thomas, F. Höök, G. Fragneto, F. Tiberg, and T. Nylander, Soft Matter **4**, 2267 (2008).
[26]H. P. Vacklin, F. Tiberg, and R. K. Thomas, Biochim. Biophys. Acta **1668**, 17 (2005).
[27]H. P. Vacklin, F. Tiberg, G. Fragneto, and R. K. Thomas, Langmuir **21**, 2827 (2005).
[28]A. Yaseen, J. R. Lu, J. R. P. Webster, and J. Penfold, Biophys. Chem. **117**, 263 (2005).
[29]A. P. Le Brun, S. A. Holt, D. S. Shah, C. F. Majkrzak, and J. H. Lakey, Eur. Biophys. J. **37**, 639 (2008).
[30]L. Nevot and P. Croce, Rev. Phys. Appl. **15**, 761 (1980).
[31]See http://www.hmi.de/bensc/instrumentation/instrumente/v6/refl/parratt_en.htm for a description of the computer programs and access to the software.
[32]See http://material.fysik.uu.se/Group_members/adrian/reflect.htm# Analysis for a description of the computer programs and access to the software.
[33]A. Nelson, J. Appl. Crystallogr. **39**, 273 (2006).
[34]M. Björck and G. Andersson, J. Appl. Crystallogr. **40**, 1174 (2007).
[35]See http://material.fysik.uu.se/Group_members/adrian/cprof.htm for an account of the specific computer programs.
[36]See http://material.fysik.uu.se/Group_members/adrian/refprog.htm for an account of the specific computer programs.
[37]J. Penfold, D. S. Sivia, E. Staples, I. Tucker, and R. K. Thomas, Langmuir **20**, 2265 (2004).
[38]T. P. Russell, Physica B (Amsterdam) **221**, 267 (1996).
[39]J. Zhang, T. Nylander, R. A. Campbell, A. R. Rennie, S. Zauscher, and P. Linse, Soft Matter **4**, 500 (2008).
[40]J. M. H. M. Scheutjens and G. J. Fleer, J. Phys. Chem. **83**, 1619 (1979).
[41]G. J. Fleer, M. A. Cohen Stuart, J. M. H. M. Scheutjens, T. Cosgrove, and B. Vincent, *Polymers at Interfaces* (Chapman & Hall, London, 1993).
[42]P. J. Flory, *Principles of Polymer Chemistry* (Cornell University Press, Ithaca, NY, 1953).
[43]G. Karlström, J. Phys. Chem. **89**, 4962 (1985).
[44]P. Linse and M. Björling, Macromolecules **24**, 6700 (1991).
[45]P. Linse and T. A. Hatton, Langmuir **13**, 4066 (1997).
[46]J. E. Dennis, Jr. and R. B. Schnabel, *Numerical Methods for Unconstrained Optimization and Nonlinear Equations* (Prentice-Hall, Englewood Cliffs, 1983).
[47]M. Landgren and B. Jonsson, J. Phys. Chem. **97**, 1656 (1993).
[48]R. M. Azzam and N. M. Bashara, *Ellipsometry and Polarized Light* (North-Holland, Amsterdam, 1977).
[49]J. A. Defeijter, J. Benjamins, and F. A. Veer, Biopolymers **17**, 1759 (1978).
[50]M. Rodahl, F. Hook, C. Fredriksson, C. A. Keller, A. Krozer, P. Brzezinski, M. Voinova, and B. Kasemo, Faraday Discuss. **107**, 229 (1997).
[51]F. Höök, B. Kasemo, T. Nylander, C. Fant, K. Sott, and E. H. Elwing, Anal. Chem. **73**, 5796 (2001).
[52]J. S. Pedersen, Adv. Colloid Interface Sci. **70**, 171 (1997).
[53]A. D. Bangham and R. W. Horne, J. Mol. Biol. **8**, 660 (1964).
[54]G. Gregoriadis, C. P. Swain, E. J. Wills, and A. S. Tavill, Lancet **303**, 1313 (1974).
[55]P. Couvreur and C. Vauthier, Pharm. Res. **23**, 1417 (2006).
[56]S. Ganta, H. Devalapally, A. Shahiwala, and M. Amiji, J. Controlled Release **126**, 187 (2008).
[57]M. C. Woodle and D. D. Lasic, Biochim. Biophys. Acta **1113**, 171 (1992).
[58]D. Papahadjopoulos *et al.*, Proc. Natl. Acad. Sci. U.S.A. **88**, 11460 (1991).
[59]S. I. Jeon, J. H. Lee, J. D. Andrade, and P. G. De Gennes, J. Colloid Interface Sci. **142**, 149 (1991).
[60]L. M. Ickenstein, M. C. Arfvidsson, D. Needham, L. D. Mayera, and K. Edwards, Biochim. Biophys. Acta **1614**, 135 (2003).
[61]J. S. Patton and M. C. Carey, Science **204**, 145 (1979).
[62]K. Larsson, J. Phys. Chem. **93**, 7304 (1989).
[63]W. Buchheim and K. Larsson, J. Colloid Interface Sci. **117**, 582 (1987).
[64]M. Monduzzi, H. Ljusberg-Wahren, and K. Larsson, Langmuir **16**, 7355 (2000).
[65]K. Larsson, Curr. Opin. Colloid Interface Sci. **5**, 64 (2000).
[66]T. Landh, J. Phys. Chem. **98**, 8453 (1994).
[67]J. Gustafsson, H. Ljusberg-Wahren, M. Almgren, and K. Larsson, Langmuir **12**, 4611 (1996).
[68]J. Barauskas, M. Johnsson, F. Johnson, and F. Tiberg, Langmuir **21**, 2569 (2005).
[69]J. Barauskas, M. Johnsson, and F. Tiberg, Nano Lett. **5**, 1615 (2005).
[70]*Delivery and Controlled Release of Bioactives in Foods and Nutraceuticals*, edited by N. Garti (Woodhead, Cambridge, 2008).
[71]E. Acosta, in *Delivery and Controlled Release of Bioactives in Foods and Nutraceuticals*, edited by N. Garti (Woodhead, Cambridge, 2008), pp. 53–106.
[72]T. Niidome and L. Huang, Gene Ther. **9**, 1647 (2002).
[73]K. K. Ewert, C. E. Samuel, and C. R. Safinya, in *DNA Interactions with*

Polymers and Surfactants, edited by R. Dias and B. Lindman (Wiley, Hoboken, NJ, 2008), pp. 377–404.
[74]E. Sackmann, Science **271**, 43 (1996).
[75]R. P. Richter, R. Berat, and A. R. Brisson, Langmuir **22**, 3497 (2006).
[76]F. Tiberg, I. Harwigsson, and M. Malmsten, Eur. Biophys. J. **29**, 196 (2000).
[77]T. Gutberlet, R. Steitz, G. Fragneto, and B. Klösgen, J. Phys.: Condens. Matter **16**, S2469 (2004).
[78]D. Stroumpoulis, A. Parra, and M. Tirrell, AIChE J. **52**, 2931 (2006).
[79]C. A. Keller and B. Kasemo, Biophys. J. **75**, 1397 (1998).
[80]H. P. Wacklin and R. K. Thomas, Langmuir **23**, 7644 (2007).
[81]L. M. Grant and F. Tiberg, Biophys. J. **82**, 1373 (2002).
[82]J. Y. Wong, J. Majewski, M. Seitz, C. K. Park, J. N. Israelachvili, and G. S. Smith, Biophys. J. **77**, 1445 (1999).
[83]U. A. Perez-Salas, K. M. Faucher, C. F. Majkrzak, N. F. Berk, S. Krueger, and E. L. Chaikof, Langmuir **19**, 7688 (2003).
[84]M. Tanaka and E. Sackmann, Nature (London) **437**, 656 (2005).
[85]G. Valincius, D. J. McGillivray, W. Febo-Ayala, D. J. Vanderah, J. J. Kasianowicz, and M. Lösche, J. Phys. Chem. B **110**, 10213 (2006).
[86]D. J. McGillivray, G. Valincius, D. J. Vanderah, W. Febo-Ayala, J. T. Woodward, F. Heinrich, J. J. Kasianowicz, and M. Lösche, BioInterphases **2**, 21 (2007).
[87]B. A. Cornell, V. L. B. Braach-Maksvytis, L. G. King, P. D. J. Osman, B. Raguse, L. Wieczorek, and R. J. Pace, Nature (London) **387**, 580 (1997).
[88]D. A. Doshi, A. M. Dattelbaum, E. B. Watkins, C. J. Brinker, B. I. Swanson, A. P. Shreve, A. N. Parikh, and J. Majewski, Langmuir **21**, 2865 (2005).
[89]A. V. Hughes, J. R. Howse, A. Dabkowska, R. A. L. Jones, M. J. Lawrence, and S. J. Roser, Langmuir **24**, 1989 (2008).
[90]H. Haas, R. Steitz, A. Fasano, G. M. Liuzzi, E. Polverini, P. Cavatorta, and P. Riccio, Langmuir **23**, 8491 (2007).
[91]G. Fragneto and M. Rheinstädter, C. R. Phys. **8**, 865 (2007).
[92]C. Li, D. Constantin, and T. Salditt, J. Phys.: Condens. Matter **16**, S2439 (2004).
[93]N. Kucerka, M.-P. Nieh, J. Pencer, T. Harroun, and J. Katsaras, Curr. Opin. Colloid Interface Sci. **12**, 17 (2007).
[94]P. Callow, G. Fragneto, R. Cubitt, D. J. Barlow, M. J. Lawrence, and P. Timmins, Langmuir **21**, 7912 (2005).
[95]G. Wagner, A. Bancaud, J.-P. Quivy, C. Clapier, G. Almouzni, and J.-L. Viovy, Biophys. J. **89**, 3647 (2005).
[96]K. Matsubara, N. Sano, T. Umehara, and M. Horikoshi, Genes Cells **12**, 13 (2007).
[97]A. Bertin, A. Leforestier, D. Durand, and F. Livolant, Biochemistry **43**, 4773 (2004).
[98]S. A. Gani, D. C. Mukherjee, and D. K. Chattoraj, Langmuir **15**, 7130 (1999).
[99]A. Elaissari, P. Cros, C. Pichot, V. Laurent, and B. Mandrand, Colloids Surf., A **83**, 25 (1994).
[100]V. Balladur, A. Theretz, and B. Mandrand, J. Colloid Interface Sci. **194**, 408 (1997).
[101]R. R. Kunze and R. R. Netz, Phys. Rev. Lett. **85**, 4389 (2000).
[102]I. M. Verma and N. Somia, Nature (London) **389**, 239 (1997).
[103]N. S. Templeton and D. D. Lasic, Mol. Biotechnol. **11**, 175 (1999).
[104]D. K. Chattoraj, P. Chowrashi, and K. Chakravarti, Biopolymers **5**, 173 (1967).
[105]K. Eskilsson, C. Leal, B. Lindman, M. Miguel, and T. Nylander, Langmuir **17**, 1666 (2001).
[106]M. Cárdenas, K. Schillen, T. Nylander, J. Jansson, and B. Lindman, Phys. Chem. Chem. Phys. **6**, 1603 (2004).
[107]M. Cárdenas, A. Braem, T. Nylander, and B. Lindman, Langmuir **19**, 7712 (2003).
[108]L. Stryer, *Biochemistry* (Freeman, New York, 1995).
[109]A. Elaissari, Y. Chevalier, F. Ganachaud, T. Delair, and C. Pichot, Langmuir **16**, 1261 (2000).
[110]D. Zanchet, C. M. Michel, W. J. Parak, D. Gerion, and A. P. Alivisatos, Nano Lett. **1**, 32 (2001).
[111]S. J. Park, A. A. Lazarides, J. J. Storhoff, L. Pesce, and C. A. Mirkin, J. Phys. Chem. B **108**, 12375 (2004).
[112]L. Olofsson, T. Rindzevicius, I. Pfeiffer, M. Käll, and F. Höök, Langmuir **19**, 10414 (2003).
[113]S. Moses *et al.*, Langmuir **20**, 11134 (2004).
[114]R. Levicky, T. M. Herne, M. J. Tarlov, and S. K. Satija, J. Am. Chem. Soc. **120**, 9787 (1998).
[115]C.-Y. Lee, P. Gong, G. M. Harbers, D. W. Grainger, D. G. Castner, and L. J. Gamble, Anal. Chem. **78**, 3316 (2006).
[116]P. Gong, C.-Y. Lee, L. J. Gamble, D. G. Castner, and D. W. Grainger, Anal. Chem. **78**, 3326 (2006).
[117]L. M. Demers, C. A. Mirkin, R. C. Mucic, R. A. Reynolds, R. L. Letsinger, R. Elghanian, and G. Viswanadham, Anal. Chem. **72**, 5535 (2000).
[118]S. M. Mel'nikov, V. G. Sergeyev, and K. Yoshikawa, J. Am. Chem. Soc. **117**, 9951 (1995).
[119]R. Dias, S. Mel'nikov, B. Lindman, and M. G. Miguel, Langmuir **16**, 9577 (2000).
[120]M. Cárdenas, T. Nylander, R. K. Thomas, and B. Lindman, Langmuir **21**, 6495 (2005).
[121]J. Zhang, D. J. F. Taylor, P. X. Li, R. K. Thomas, J. B. Wang, and J. Penfold, Langmuir **24**, 1863 (2008).
[122]J.-C. Wu, T.-L. Lin, U.-S. Jeng, and N. Torikai, Physica B (Amsterdam) **385–386**, 838 (2006).
[123]J.-C. Wu, T.-L. Lin, U.-S. Jeng, H.-Y. Lee, and T. Gutberlet, Physica B (Amsterdam) **385–386**, 841 (2006).
[124]X. Chen, J. Wang, N. Shen, Y. Luo, L. Li, M. Liu, and R. K. Thomas, Langmuir **18**, 6222 (2002).
[125]J. Generosi, C. Castellano, D. Pozzi, A. C. Castellanon, R. Felici, F. Natali, and G. Fragneto, J. Appl. Phys. **96**, 6839 (2004).
[126]P. T. Spicer, Curr. Opin. Colloid Interface Sci. **10**, 274 (2005).
[127]L. Sagalowicz, R. Mezzenga, and M. E. Leser, Curr. Opin. Colloid Interface Sci. **11**, 224 (2006).
[128]P. Vandoolaeghe, F. Tiberg, and T. Nylander, Langmuir **22**, 9169 (2006).
[129]M. Cárdenas, J. Campos-Teran, T. Nylander, and B. Lindman, Langmuir **20**, 8597 (2004).
[130]R. Bruinsma, Eur. Phys. J. B **4**, 75 (1998).
[131]R. Chatterjee and D. K. Chattoraj, Biopolymers **18**, 147 (1979).